

Angular Analysis of the Decay $\Lambda_b \rightarrow \Lambda(\rightarrow N\pi)\ell^+\ell^-$

Philipp Böer, Thorsten Feldmann, Danny van Dyk

*Theoretische Physik 1, Naturwissenschaftlich-Technische Fakultät, Universität Siegen,
Walter-Flex-Straße 3, D-57068 Siegen, Germany*

E-mail: boeer@physik.uni-siegen.de, thorsten.feldmann@uni-siegen.de,
vandyk@physik.uni-siegen.de

ABSTRACT: We study the differential decay rate for the rare $\Lambda_b \rightarrow \Lambda(\rightarrow N\pi)\ell^+\ell^-$ transition, including a determination of the complete angular distribution, assuming unpolarized Λ_b baryons. On the basis of a properly chosen parametrization of the various helicity amplitudes, we provide expressions for the angular observables within the Standard Model and a subset of new physics models with chirality-flipped operators. Hadronic effects at low recoil are estimated by combining information from lattice QCD with (improved) form-factor relations in Heavy Quark Effective Theory. Our estimates for large hadronic recoil – at this stage – are still rather uncertain because the baryonic input functions are not so well known, and non-factorizable spectator effects have not been worked out systematically so far. Still, our phenomenological analysis of decay asymmetries and angular observables for $\Lambda_b \rightarrow \Lambda(\rightarrow N\pi)\ell^+\ell^-$ reveals that this decay mode can provide new and complementary constraints on the Wilson coefficients in radiative and semileptonic $b \rightarrow s$ transitions compared to the corresponding mesonic modes.

KEYWORDS: Rare Quark Decays, Heavy Quark Expansion, Soft-Collinear Effective Theory, Baryonic Form Factors

Contents

1	Introduction	1
2	Effective Hamiltonian for $b \rightarrow s\ell^+\ell^-$ Transitions	3
3	The Decays $\Lambda_b \rightarrow \Lambda(\rightarrow N\pi)\ell^+\ell^-$	4
3.1	Kinematics	4
3.2	Hadronic Matrix Elements	5
3.2.1	$\Lambda_b \rightarrow \Lambda$ Helicity Form Factors	5
3.2.2	Hadronic Couplings in $\Lambda \rightarrow N\pi$	7
3.3	Angular Observables	9
4	Phenomenological Applications	10
4.1	Simple Observables	10
4.2	Exploiting Form-Factor Symmetries at Low Recoil	11
4.3	Simplifications at Large Recoil	14
4.4	Numerical Analysis	16
4.4.1	Transition Form Factors	16
4.4.2	Results	17
5	Summary and Outlook	19
A	Corrections to HQET Form Factor Relations	20
B	Form Factor Parametrisation	22
C	Statistical Analysis of the Transition Form Factors	23
D	Details on the Kinematics	26
D.1	Λ_b Rest Frame	26
D.2	Dilepton Rest Frame	27
D.3	$N\pi$ System	27
E	Explicit Spinor Representations	28

1 Introduction

Rare decays based on radiative or semi-leptonic $b \rightarrow s$ transitions offer various possibilities to test the predictions for flavour-changing neutral currents (FCNCs) in the Standard Model (SM) against new physics (NP) extensions (for comprehensive summaries of theoretical and experimental aspects, see e.g. [1–3]). In the past – notably during the “ B -factory”

era [4] – the main phenomenological focus was on inclusive distributions ($B \rightarrow X_s \gamma$ and $B \rightarrow X_s \ell^+ \ell^-$) or exclusive decay observables (e.g. in $B \rightarrow K^* \gamma$, $B \rightarrow K^{(*)} \ell^+ \ell^-$, ...) for mesonic decays. With the recent b -physics program at LHC (and here, in particular, the dedicated LHCb experiment) not only more precise measurements of radiative B - and B_s -meson decays, but also information on baryonic modes like $\Lambda_b \rightarrow \Lambda \ell^+ \ell^-$ with reasonable accuracy will become available [5]. (For an incomplete list of previous phenomenological studies, see e.g. [6–10] and references therein).

Exclusive hadronic decays, by definition, are theoretically challenging because the calculation of decay amplitudes induces a number of hadronic uncertainties related to long-distance QCD dynamics. For $b \rightarrow s \ell^+ \ell^-$ transitions this includes hadronic transition form factors, which parametrize the “naively” factorizing contributions from $b \rightarrow s \gamma$ and $b \rightarrow s \ell^+ \ell^-$ operators. In addition, systematic uncertainties related to non-factorizable effects appear, where the short-distance dynamics is induced by *hadronic* $b \rightarrow s$ operators, while the radiation of the photon or charged lepton pair is linked to the long-distance hadronic transition. Baryonic transitions, at first glance, seem to suffer from even larger hadronic uncertainties than their mesonic counterparts since transition form factors and hadronic wave functions are only poorly known, and the analysis of the spectator dynamics is more complicated [11]. Recent progress with respect to $\Lambda_b \rightarrow \Lambda$ form factors includes lattice-QCD results in the heavy-mass limit [12] (valid at low and intermediate recoil), and a sum-rule analysis of spectator-scattering corrections to form factor relations at large recoil [13]. Also, a better theoretical understanding of the Λ_b wave function (in the form of light-cone distribution amplitudes) has been achieved recently [14–16].

However, as we will also argue in this paper, exclusive modes like $\Lambda_b \rightarrow \Lambda \ell^+ \ell^-$ do provide interesting phenomenological potential. Exploiting the full set of angular observables that can be derived from the analysis of the subsequent $\Lambda \rightarrow N \pi$ decay, one may obtain information on the underlying short-distance weak interactions that is complementary to the analogous mesonic decay observables (see e.g. [17–23]). This is mainly a consequence of the fact that the subsequent weak decay $\Lambda \rightarrow N \pi$ is parity violating, while the strong decay $K^* \rightarrow K \pi$ in the mesonic counterpart case, $B \rightarrow K^* \ell^+ \ell^-$, is not.¹ Furthermore, within such an analysis, independent information on the hadronic parameters themselves can be extracted from experimental data. In particular, form-factor relations that arise in the infinite-mass limit for the heavy b -quark, can be tested (notice that the number of independent form factors for $\Lambda_b \rightarrow \Lambda$ transitions in that limit is smaller than for $B \rightarrow K^*$ transitions: 2 at low recoil [24], and one at large recoil [13, 25]).

The outline of this paper is as follows. In the next section, we will briefly summarize our notation and conventions regarding the short-distance operator basis in the weak effective Hamiltonian. In section 3 we derive the necessary expressions to describe the $\Lambda_b \rightarrow \Lambda(\rightarrow N \pi) \ell^+ \ell^-$ differential decay rate.² To this end, we define the relevant kinematic

¹The background from direct $\Lambda_b \rightarrow N \pi \ell^+ \ell^-$ decays is expected to be low: First, the direct decay is relatively suppressed by $|V_{td}/V_{ts}|$. Second, the signal with an intermediate Λ baryon can be distinguished by requiring a sizable displacement between the $\Lambda_b \ell^+ \ell^-$ and $N \pi$ decay vertices.

²We will restrict ourselves to the case of unpolarized Λ_b baryons, as the Λ_b polarization in the LHCb setup has been measured to be small [26], and polarization effects in the symmetric ATLAS and CMS

variables, define the general set of $\Lambda_b \rightarrow \Lambda$ form factors in the helicity basis, and discuss the hadronic couplings appearing in the $\Lambda \rightarrow N\pi$ decay. From this we derive expressions for the angular observables in terms of transversity amplitudes. Section 4 is dedicated to the phenomenological analysis of interesting observables. Specifically, we consider the fraction of transverse dilepton polarization, the leptonic, baryonic and mixed forward-backward asymmetries, and a number of certain ratios of angular observables where either short-distance effects or form-factor uncertainties drop out to first approximation. We also work out the simplifications that arise from the heavy-quark expansion at low or large recoil. We conclude this section with numerical predictions for a selection of observables, making use of the available theoretical and phenomenological information on the relevant input parameters, and compare to presently available experimental data in the low-recoil region. We conclude with a summary and outlook. Some technical details are summarized in the appendices.

2 Effective Hamiltonian for $b \rightarrow s\ell^+\ell^-$ Transitions

The effective weak Hamiltonian for $b \rightarrow s\ell^+\ell^-$ transitions ($|\Delta B| = |\Delta S| = 1$) in the SM (see e.g. [27–29]) contains radiative ($b \rightarrow s\gamma$) and semi-leptonic ($b \rightarrow s\ell^+\ell^-$) operators as well as hadronic operators ($b \rightarrow sq\bar{q}$, $b \rightarrow sg$). For the radiative and semileptonic operators, we find it convenient to use the normalization convention

$$\mathcal{H}^{\text{eff}}\Big|_{\text{SM,naive}} = \underbrace{\frac{4G_{\text{F}}}{\sqrt{2}} V_{tb}V_{ts}^* \frac{\alpha_e}{4\pi}}_{N_1} \sum_{i=7,9,10} \mathcal{C}_i(\mu) \mathcal{O}_i, \quad (2.1)$$

with the SM operators

$$\mathcal{O}_{7(\prime)} = \frac{m_b}{e} [\bar{s}\sigma^{\mu\nu} P_{R(L)} b] F_{\mu\nu}, \quad \mathcal{O}_9 = [\bar{s}\gamma^\mu P_L b] [\bar{\ell}\gamma_\mu \ell], \quad \mathcal{O}_{10} = [\bar{s}\gamma^\mu P_L b] [\bar{\ell}\gamma_\mu \gamma_5 \ell]. \quad (2.2)$$

For simplicity, we only take into account the factorizable quark-loop contributions of the hadronic operators \mathcal{O}_{1-6} and \mathcal{O}_8^g , which can be lumped into effective Wilson coefficients $\mathcal{C}_7^{\text{eff}}$ and $\mathcal{C}_9^{\text{eff}}(q^2)$. We ignore non-factorizable effects, which are expected to play a non-negligible role, particularly at large hadronic recoil [30, 31].

Notice that the radiative operators $\mathcal{O}_{7(\prime)}$ contribute to the semi-leptonic decay through photon exchange and its electromagnetic coupling to a lepton pair such that

$$\langle \Lambda(k)\ell^+(q_1)\ell^-(q_2) | \mathcal{O}_{7(\prime)} | \Lambda_b(p) \rangle = -\frac{2m_b}{q^2} \langle \Lambda | \bar{s} i\sigma^{\mu\nu} q_\nu P_{R(L)} b | \Lambda_b \rangle [\bar{u}_\ell \gamma_\mu v_\ell], \quad (2.3)$$

with $q^\mu = p^\mu - k^\mu$ being the momentum transfer to the lepton pair. In this notation the Wilson coefficient $\mathcal{C}_{7'}$ is suppressed by m_s/m_b in the SM.

Potential NP contributions to $b \rightarrow s\gamma$ and $b \rightarrow s\ell^+\ell^-$, on the one hand, modify the Wilson coefficients of the SM operators above and, on the other hand, feed into new effective operators,

$$\mathcal{H}^{\text{eff}}\Big|_{\text{NP,naive}} = N_1 \sum_{i=S(\prime),P(\prime),9',10',T,T5} \mathcal{C}_i(\mu) \mathcal{O}_i. \quad (2.4)$$

detectors will average out.

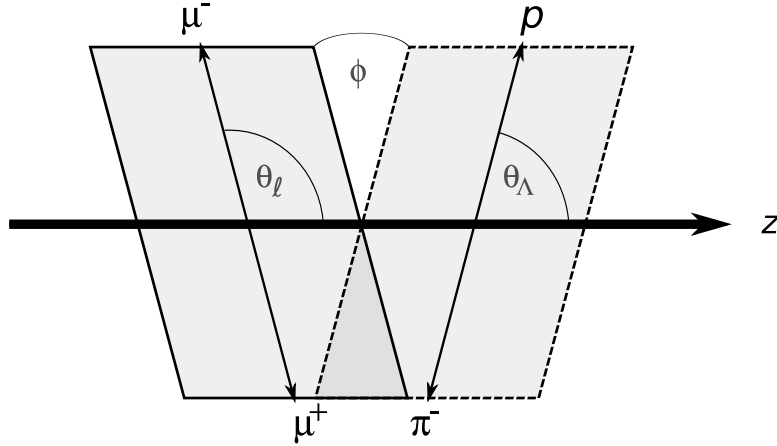


Figure 1. Topology of the decay $\Lambda_b \rightarrow \Lambda (\rightarrow p\pi^-) \ell^+ \ell^-$.

Here the SM operators are completed to form a basis of dimension-six operators by:

$$\begin{aligned}
\mathcal{O}_{S^{(\prime)}} &= [\bar{s}P_{R(L)}b][\bar{\ell}\ell], & \mathcal{O}_{P^{(\prime)}} &= [\bar{s}P_{R(L)}b][\bar{\ell}\gamma_5\ell], \\
\mathcal{O}_{9'} &= [\bar{s}\gamma^\mu P_R b][\bar{\ell}\gamma_\mu\ell], & \mathcal{O}_{10'} &= [\bar{s}\gamma^\mu P_R b][\bar{\ell}\gamma_\mu\gamma_5\ell], \\
\mathcal{O}_T &= [\bar{s}\sigma^{\mu\nu}b][\bar{\ell}\sigma_{\mu\nu}\ell], & \mathcal{O}_{T5} &= \frac{i}{2}\varepsilon_{\mu\nu\alpha\beta}[\bar{s}\sigma^{\mu\nu}b][\bar{\ell}\sigma^{\alpha\beta}\ell],
\end{aligned} \tag{2.5}$$

which contains the chirality-flipped counterparts of the SM operators \mathcal{O}_9 and \mathcal{O}_{10} together with scalar, pseudoscalar, tensor and pseudotensor operators.

3 The Decays $\Lambda_b \rightarrow \Lambda (\rightarrow N\pi)\ell^+\ell^-$

3.1 Kinematics

We assign particle momenta and spin variables for the baryonic states in the decay according to:

$$\begin{aligned}
\Lambda_b(p, s_{\Lambda_b}) &\rightarrow \Lambda(k, s_\Lambda) \ell^+(q_1) \ell^-(q_2), \\
\Lambda(k, s_\Lambda) &\rightarrow N(k_1, s_N) \pi(k_2), \quad (N\pi = \{p\pi^-, n\pi^0\}).
\end{aligned} \tag{3.1}$$

Here, s_i are the projections of the baryonic spins onto the z -axis in their rest frames. It is convenient to define sums and differences of the hadronic and leptonic momenta in the final state,

$$q^\mu = q_1^\mu + q_2^\mu, \quad \bar{q}^\mu = q_1^\mu - q_2^\mu, \quad k^\mu = k_1^\mu + k_2^\mu, \quad \bar{k}^\mu = k_1^\mu - k_2^\mu. \tag{3.2}$$

The discussion of the kinematics is similar to what has been already worked out for semileptonic four-body B -meson decays, see e.g. [17, 18, 32–34]. We end up with four independent kinematic variables, which can be chosen as the invariant mass q^2 , the helicity angles θ_Λ

and θ_ℓ , and the azimuthal angle ϕ , see Fig. 1, which are defined in the relevant Lorentz frames in appendix D.

Furthermore, we introduce a set of virtual polarization vectors $\varepsilon^\mu(\lambda = t, +, -, 0)$ with $q \cdot \varepsilon(\pm) = q \cdot \varepsilon(0) = 0$, which in the dilepton rest frame take the canonical form as shown in appendix D. In terms of the leptonic angle θ_ℓ and the relativistic lepton velocity,

$$\beta_\ell = \sqrt{1 - \frac{4m_\ell^2}{q^2}},$$

the polarization vectors obey

$$\bar{q} \cdot \varepsilon(t) = 0, \quad \bar{q} \cdot \varepsilon(\pm) = \pm \frac{\beta_\ell}{\sqrt{2}} \sqrt{q^2} \sin \theta_\ell, \quad \bar{q} \cdot \varepsilon(0) = -\beta_\ell \sqrt{q^2} \cos \theta_\ell. \quad (3.3)$$

Similarly, the corresponding hadronic kinematic variables appear in the following Lorentz-scalar products,

$$\varepsilon^*(t) \cdot \bar{k} = \frac{\beta_{N\pi}}{2} \sqrt{\lambda} \cos \theta_\Lambda, \quad \varepsilon^*(\pm) \cdot \bar{k} = \pm \frac{\beta_{N\pi}}{\sqrt{2}} m_\Lambda \sin \theta_\Lambda \exp(\pm i\phi). \quad (3.4)$$

Here, we abbreviate $\lambda \equiv \lambda(m_{\Lambda_b}^2, m_\Lambda^2, q^2)$, with the Källén function

$$\lambda(a, b, c) = a^2 + b^2 + c^2 - 2(ab + ac + bc). \quad (3.5)$$

We also define

$$\beta_{N\pi} = \frac{\sqrt{\lambda(m_\Lambda^2, m_N^2, m_\pi^2)}}{m_\Lambda^2}. \quad (3.6)$$

3.2 Hadronic Matrix Elements

3.2.1 $\Lambda_b \rightarrow \Lambda$ Helicity Form Factors

The hadronic form factors for $\Lambda_b \rightarrow \Lambda$ transitions are most conveniently defined in the helicity basis [13]. For the vector current, this yields three independent helicity form factors $f_i^V(q^2)$, entering the corresponding helicity amplitudes $H_i^V(s_{\Lambda_b}, s_\Lambda)$,

$$\begin{aligned} H_t^V(s_{\Lambda_b}, s_\Lambda) &\equiv \varepsilon_\mu^*(t) \langle \Lambda(k, s_\Lambda) | \bar{s} \gamma^\mu b | \Lambda_b(p, s_{\Lambda_b}) \rangle \\ &= f_t^V(q^2) \frac{m_{\Lambda_b} - m_\Lambda}{\sqrt{q^2}} [\bar{u}(k, s_\Lambda) u(p, s_{\Lambda_b})], \\ H_0^V(s_{\Lambda_b}, s_\Lambda) &\equiv \varepsilon_\mu^*(0) \langle \Lambda(k, s_\Lambda) | \bar{s} \gamma^\mu b | \Lambda_b(p, s_{\Lambda_b}) \rangle \\ &= 2 f_0^V(q^2) \frac{m_{\Lambda_b} + m_\Lambda}{s_+} (k \cdot \varepsilon^*(0)) [\bar{u}(k, s_\Lambda) u(p, s_{\Lambda_b})], \\ H_\pm^V(s_{\Lambda_b}, s_\Lambda) &\equiv \varepsilon_\mu^*(\pm) \langle \Lambda(k, s_\Lambda) | \bar{s} \gamma^\mu b | \Lambda_b(p, s_{\Lambda_b}) \rangle \\ &= f_\pm^V(q^2) [\bar{u}(k, s_\Lambda) \not{\varepsilon}^*(\pm) u(p, s_{\Lambda_b})], \end{aligned} \quad (3.7)$$

where we slightly changed notation compared to [13]. The kinematic functions s_\pm are defined as

$$s_\pm \equiv (m_{\Lambda_b} \pm m_\Lambda)^2 - q^2. \quad (3.8)$$

Analogous expressions are obtained for the axial-vector current,

$$\begin{aligned}
H_t^A(s_{\Lambda_b}, s_\Lambda) &\equiv \varepsilon_\mu^*(t) \langle \Lambda(k, s_\Lambda) | \bar{s} \gamma^\mu \gamma_5 b | \Lambda_b(p, s_{\Lambda_b}) \rangle \\
&= -f_t^A(q^2) \frac{m_{\Lambda_b} + m_\Lambda}{\sqrt{q^2}} [\bar{u}(k, s_\Lambda) \gamma_5 u(p, s_{\Lambda_b})] , \\
H_0^A(s_{\Lambda_b}, s_\Lambda) &\equiv \varepsilon_\mu^*(0) \langle \Lambda(k, s_\Lambda) | \bar{s} \gamma^\mu \gamma_5 b | \Lambda_b(p, s_{\Lambda_b}) \rangle \\
&= -2 f_0^A(q^2) \frac{m_{\Lambda_b} - m_\Lambda}{s_-} (k \cdot \varepsilon^*(0)) [\bar{u}(k, s_\Lambda) \gamma_5 u(p, s_{\Lambda_b})] , \\
H_\pm^A(s_{\Lambda_b}, s_\Lambda) &\equiv \varepsilon_\mu^*(\pm) \langle \Lambda(k, s_\Lambda) | \bar{s} \gamma^\mu \gamma_5 b | \Lambda_b(p, s_{\Lambda_b}) \rangle \\
&= f_\pm^A(q^2) [\bar{u}(k, s_\Lambda) \not{\varepsilon}^*(\pm) \gamma_5 u(p, s_{\Lambda_b})] . \tag{3.9}
\end{aligned}$$

Restricting ourselves to the SM operator basis and its flipped counterpart, only the q^ν projections of the tensor and pseudotensor currents appears, which lead to another four independent form factors,

$$\begin{aligned}
H_0^T(s_{\Lambda_b}, s_\Lambda) &\equiv \varepsilon_\mu^*(0) \langle \Lambda(k, s_\Lambda) | \bar{s} i \sigma^{\mu\nu} q_\nu b | \Lambda_b(p, s_{\Lambda_b}) \rangle \\
&= -2 f_0^T(q^2) \frac{q^2}{s_+} (k \cdot \varepsilon^*(0)) [\bar{u}(k, s_\Lambda) u(p, s_{\Lambda_b})] , \\
H_\pm^T(s_{\Lambda_b}, s_\Lambda) &\equiv \langle \Lambda(k, s_\Lambda) | \bar{s} i \sigma^{\mu\nu} q_\nu b | \Lambda_b(p, s_{\Lambda_b}) \rangle \varepsilon_\mu^*(\pm) \\
&= -f_\pm^T(q^2) (m_{\Lambda_b} + m_\Lambda) [\bar{u}(k, s_\Lambda) \not{\varepsilon}^*(\pm) u(p, s_{\Lambda_b})] , \tag{3.10}
\end{aligned}$$

and

$$\begin{aligned}
H_0^{T5}(s_{\Lambda_b}, s_\Lambda) &\equiv \varepsilon_\mu^*(0) \langle \Lambda(k, s_\Lambda) | \bar{s} i \sigma^{\mu\nu} q_\nu \gamma_5 b | \Lambda_b(p, s_{\Lambda_b}) \rangle \\
&= -2 f_0^{T5}(q^2) \frac{q^2}{s_-} (k \cdot \varepsilon^*(0)) [\bar{u}(k, s_\Lambda) \gamma_5 u(p, s_{\Lambda_b})] , \\
H_\pm^{T5}(s_{\Lambda_b}, s_\Lambda) &\equiv \varepsilon_\mu^*(\pm) \langle \Lambda(k, s_\Lambda) | \bar{s} i \sigma^{\mu\nu} q_\nu \gamma_5 b | \Lambda_b(p, s_{\Lambda_b}) \rangle \\
&= f_\pm^{T5}(q^2) (m_{\Lambda_b} - m_\Lambda) [\bar{u}(k, s_\Lambda) \not{\varepsilon}^*(\pm) \gamma_5 u(p, s_{\Lambda_b})] . \tag{3.11}
\end{aligned}$$

The spinor matrix elements for given combinations of spin orientations are summarized in appendix E. For the nonzero helicity amplitudes, we then obtain in case of the vector current

$$\begin{aligned}
H_t^V(+1/2, +1/2) &= H_t^V(-1/2, -1/2) = f_t^V(q^2) \frac{m_{\Lambda_b} - m_\Lambda}{\sqrt{q^2}} \sqrt{s_+} , \\
H_0^V(+1/2, +1/2) &= H_0^V(-1/2, -1/2) = f_0^V(q^2) \frac{m_{\Lambda_b} + m_\Lambda}{\sqrt{q^2}} \sqrt{s_-} , \\
H_+^V(-1/2, +1/2) &= H_-^V(+1/2, -1/2) = -f_\pm^V(q^2) \sqrt{2s_-} . \tag{3.12}
\end{aligned}$$

Similarly, in case of the axial-vector current we have

$$\begin{aligned}
H_t^A(+1/2, +1/2) &= -H_t^A(-1/2, -1/2) = f_t^A(q^2) \frac{m_{\Lambda_b} + m_\Lambda}{\sqrt{q^2}} \sqrt{s_-} , \\
H_0^A(+1/2, +1/2) &= -H_0^A(-1/2, -1/2) = f_0^A(q^2) \frac{m_{\Lambda_b} - m_\Lambda}{\sqrt{q^2}} \sqrt{s_+} , \\
H_+^A(-1/2, +1/2) &= -H_-^A(+1/2, -1/2) = -f_\pm^A(q^2) \sqrt{2s_+} . \tag{3.13}
\end{aligned}$$

For the tensor and pseudotensor currents, the non-vanishing helicity amplitudes read

$$\begin{aligned} H_0^T(+1/2, +1/2) &= H_0^T(-1/2, -1/2) = -f_0^T(q^2) \sqrt{q^2} \sqrt{s_-}, \\ H_+^T(-1/2, +1/2) &= H_-^T(+1/2, -1/2) = f_\perp^T(q^2) (m_{\Lambda_b} + m_\Lambda) \sqrt{2s_-}, \end{aligned} \quad (3.14)$$

and

$$\begin{aligned} H_0^{T5}(+1/2, +1/2) &= -H_0^{T5}(-1/2, -1/2) = f_0^{T5}(q^2) \sqrt{q^2} \sqrt{s_+}, \\ H_+^{T5}(-1/2, +1/2) &= -H_-^{T5}(+1/2, -1/2) = -f_\perp^{T5}(q^2) (m_{\Lambda_b} - m_\Lambda) \sqrt{2s_+}. \end{aligned} \quad (3.15)$$

From these relations the advantage of using form factors defined in the helicity basis becomes evident.

We combine the contributions of the individual operators with the corresponding Wilson coefficients, distinguish the contributions for different lepton chiralities, and change to the transversity basis. The primary decay $\Lambda_b \rightarrow \Lambda \ell^+ \ell^-$ is then described by 8 transversity amplitudes, which we denote as

$$\begin{aligned} A_{\perp 1}^{L(R)} &= +\sqrt{2}N \left(C_{9,10,+}^{L(R)} H_+^V(-1/2, +1/2) - \frac{2m_b(\mathcal{C}_7 + \mathcal{C}_{7'})}{q^2} H_+^T(-1/2, +1/2) \right), \\ A_{\parallel 1}^{L(R)} &= -\sqrt{2}N \left(C_{9,10,-}^{L(R)} H_+^A(-1/2, +1/2) + \frac{2m_b(\mathcal{C}_7 - \mathcal{C}_{7'})}{q^2} H_+^{T5}(-1/2, +1/2) \right), \\ A_{\perp 0}^{L(R)} &= +\sqrt{2}N \left(C_{9,10,+}^{L(R)} H_0^V(+1/2, +1/2) - \frac{2m_b(\mathcal{C}_7 + \mathcal{C}_{7'})}{q^2} H_0^T(+1/2, +1/2) \right), \\ A_{\parallel 0}^{L(R)} &= -\sqrt{2}N \left(C_{9,10,-}^{L(R)} H_0^A(+1/2, +1/2) + \frac{2m_b(\mathcal{C}_7 - \mathcal{C}_{7'})}{q^2} H_0^{T5}(+1/2, +1/2) \right). \end{aligned} \quad (3.16)$$

Here, we abbreviate the various combinations of Wilson coefficients $\mathcal{C}_{9,10}$ as

$$C_{9,10,+}^{L(R)} = (\mathcal{C}_9 \mp \mathcal{C}_{10}) + (\mathcal{C}_{9'} \mp \mathcal{C}_{10'}), \quad C_{9,10,-}^{L(R)} = (\mathcal{C}_9 \mp \mathcal{C}_{10}) - (\mathcal{C}_{9'} \mp \mathcal{C}_{10'}). \quad (3.17)$$

The normalization factor N ,

$$N = N_1 \sqrt{\frac{q^2 \sqrt{\lambda(m_{\Lambda_b}^2, m_\Lambda^2, q^2)}}{3 \cdot 2^{10} m_{\Lambda_b}^3 \pi^3}} = G_F V_{tb} V_{ts}^* \alpha_e \sqrt{\frac{q^2 \sqrt{\lambda(m_{\Lambda_b}^2, m_\Lambda^2, q^2)}}{3 \cdot 2^{11} m_{\Lambda_b}^3 \pi^5}}, \quad (3.18)$$

is chosen so that $d\Gamma = \sum_\lambda |A_\lambda|^2 dq^2$. This generalizes the parametrization in terms of transversity amplitudes (for instance as described in [23]) to exclusive fermionic $b \rightarrow s \ell^+ \ell^-$ transitions.

3.2.2 Hadronic Couplings in $\Lambda \rightarrow N\pi$

In the SM the decay $\Lambda \rightarrow N\pi$ is described by the effective Hamiltonian

$$H_{\Delta S=1}^{\text{eff}} = \underbrace{\frac{4G_F}{\sqrt{2}} V_{ud}^* V_{us}}_{N_2} [\bar{d}\gamma_\mu P_L u] [\bar{u}\gamma^\mu P_L s]. \quad (3.19)$$

The hadronic matrix element which determines the $\Lambda \rightarrow N\pi$ decay can be parametrized as [35]

$$\begin{aligned} & \langle p(k_1, s_N) \pi^-(k_2) | [\bar{d} \gamma_\mu P_L u] [\bar{u} \gamma^\mu P_L s] | \Lambda(k, s_\Lambda) \rangle \\ & = [\bar{u}(k_1, s_N) (\xi \gamma_5 + \omega) u(k, s_\Lambda)] \equiv H_2(s_\Lambda, s_N). \end{aligned} \quad (3.20)$$

As a consequence of the equations of motion, only two independent hadronic parameters appear which we have denoted as ξ and ω .³ They can be extracted from the $\Lambda \rightarrow p\pi^-$ decay width and polarization measurements.

In terms of the kinematic variables introduced above (see also appendix D), the helicity amplitudes for the secondary decay can be written as

$$\begin{aligned} H_2(+1/2, +1/2) &= (\sqrt{r_+} \omega - \sqrt{r_-} \xi) \cos \frac{\theta_\Lambda}{2}, \\ H_2(+1/2, -1/2) &= (\sqrt{r_+} \omega + \sqrt{r_-} \xi) \sin \frac{\theta_\Lambda}{2} e^{i\phi}, \\ H_2(-1/2, +1/2) &= (-\sqrt{r_+} \omega + \sqrt{r_-} \xi) \sin \frac{\theta_\Lambda}{2} e^{-i\phi}, \\ H_2(-1/2, -1/2) &= (\sqrt{r_+} \omega + \sqrt{r_-} \xi) \cos \frac{\theta_\Lambda}{2}. \end{aligned} \quad (3.21)$$

where we abbreviate

$$r_\pm \equiv (m_\Lambda \pm m_N)^2 - m_\pi^2. \quad (3.22)$$

The corresponding helicity contributions to the decay width can be defined as

$$\Gamma_2(s_\Lambda^{(a)}, s_\Lambda^{(b)}) = |N_2|^2 \frac{\sqrt{r_+ r_-}}{16\pi m_\Lambda^3} \sum_{s_N} H_2(s_\Lambda^{(a)}, s_N) H_2^*(s_\Lambda^{(b)}, s_N), \quad (3.23)$$

which yield

$$\begin{aligned} \Gamma_2(+1/2, +1/2) &= (1 + \alpha \cos \theta_\Lambda) \Gamma_\Lambda, & \Gamma_2(+1/2, -1/2) &= -\alpha \sin \theta_\Lambda e^{i\phi} \Gamma_\Lambda, \\ \Gamma_2(-1/2, -1/2) &= (1 - \alpha \cos \theta_\Lambda) \Gamma_\Lambda, & \Gamma_2(-1/2, +1/2) &= -\alpha \sin \theta_\Lambda e^{-i\phi} \Gamma_\Lambda. \end{aligned} \quad (3.24)$$

Here the $\Lambda \rightarrow N\pi$ decay width is given as [35]

$$\Gamma_\Lambda = \Gamma_2(+1/2, +1/2) + \Gamma_2(-1/2, -1/2) = \frac{|N_2|^2 \sqrt{r_+ r_-}}{16\pi m_\Lambda^3} (r_- |\xi|^2 + r_+ |\omega|^2), \quad (3.25)$$

and the parity-violating decay parameter α reads

$$\alpha = \frac{-2 \operatorname{Re} \{\omega \xi\}}{\sqrt{\frac{r_-}{r_+}} |\xi|^2 + \sqrt{\frac{r_+}{r_-}} |\omega|^2} = +\alpha^{\text{exp}}. \quad (3.26)$$

³In the notation of Okun [35] our convention translates as $\omega = \alpha^{\text{Okun}}$ and $\xi = -\beta^{\text{Okun}}$. The corresponding $\Lambda \rightarrow n\pi^0$ decay parameters are related by isospin symmetry, neglecting electromagnetic and light quark-mass effects.

3.3 Angular Observables

The angular distribution for the 4-body decay can be written as a 4-fold differential decay width,

$$K(q^2, \cos \theta_\ell, \cos \theta_\Lambda, \phi) \equiv \frac{8\pi}{3} \frac{d^4\Gamma}{dq^2 d\cos \theta_\ell d\cos \theta_\Lambda d\phi}, \quad (3.27)$$

which can be decomposed in terms of a set of trigonometric functions,

$$\begin{aligned} K(q^2, \cos \theta_\ell, \cos \theta_\Lambda, \phi) = & (K_{1ss} \sin^2 \theta_\ell + K_{1cc} \cos^2 \theta_\ell + K_{1c} \cos \theta_\ell) \\ & + (K_{2ss} \sin^2 \theta_\ell + K_{2cc} \cos^2 \theta_\ell + K_{2c} \cos \theta_\ell) \cos \theta_\Lambda \\ & + (K_{3sc} \sin \theta_\ell \cos \theta_\ell + K_{3s} \sin \theta_\ell) \sin \theta_\Lambda \sin \phi \\ & + (K_{4sc} \sin \theta_\ell \cos \theta_\ell + K_{4s} \sin \theta_\ell) \sin \theta_\Lambda \cos \phi. \end{aligned} \quad (3.28)$$

Here the first line corresponds to a relative angular momentum (L, M) between the $N\pi$ system and the dilepton system of $(L, M) = (0, 0)$. The lines two to four correspond to $L = 1$, with the third component $M = 0$ in the second line, and $|M| = 1$ in lines three and four. This implies that each line of eq. (3.28) can be decomposed in terms of associated Legendre polynomials $P_l^{|M|}(\cos \theta_\ell)$, where $0 \leq l \leq 2$ holds for the dilepton angular momentum l on the basis of angular momentum conservation. This agrees exactly with our results eq. (3.28). In particular,

- (a) there are no terms $\propto \sin \theta_\ell (\cos \theta_\ell)$ or $\propto \sin \theta_\ell (\cos \theta_\ell) \cos \theta_\Lambda$,
- (b) there are no terms $\propto \sin^2 \theta_\ell \sin \theta_\Lambda$, $\propto \cos \theta_\ell \sin \theta_\Lambda$ or $\propto \cos^2 \theta_\ell \sin \theta_\Lambda$, and
- (c) no further terms can arise from dimension-six operators which are absent in our calculation; i.e., scalar and tensor operators.

The coefficients in the decomposition eq. (3.28) are referred to as angular observables and depend on the dilepton invariant mass. In our notation, they are denoted as $K_{n\lambda} \equiv K_{n\lambda}(q^2)$, with $n = 1, \dots, 4$, and $\lambda = s, c, ss, cc, sc$. In terms of the transversity amplitudes for $\Lambda_b \rightarrow \Lambda$ transitions and the decay parameter α in $\Lambda \rightarrow N\pi$ defined above, we find

$$\begin{aligned} K_{1ss}(q^2) &= \frac{1}{4} \left[|A_{\perp 1}^R|^2 + |A_{\parallel 1}^R|^2 + 2|A_{\perp 0}^R|^2 + 2|A_{\parallel 0}^R|^2 + (R \leftrightarrow L) \right], \\ K_{1cc}(q^2) &= \frac{1}{2} \left[|A_{\perp 1}^R|^2 + |A_{\parallel 1}^R|^2 + (R \leftrightarrow L) \right], \\ K_{1c}(q^2) &= -\text{Re} \left\{ A_{\perp 1}^R A_{\parallel 1}^{*R} - (R \leftrightarrow L) \right\} \end{aligned} \quad (3.29)$$

and

$$\begin{aligned} K_{2ss}(q^2) &= +\frac{\alpha}{2} \text{Re} \left\{ A_{\perp 1}^R A_{\parallel 1}^{*R} + 2A_{\perp 0}^R A_{\parallel 0}^{*R} + (R \leftrightarrow L) \right\}, \\ K_{2cc}(q^2) &= +\alpha \text{Re} \left\{ A_{\perp 1}^R A_{\parallel 1}^{*R} + (R \leftrightarrow L) \right\}, \\ K_{2c}(q^2) &= -\frac{\alpha}{2} \left[|A_{\perp 1}^R|^2 + |A_{\parallel 1}^R|^2 - (R \leftrightarrow L) \right], \end{aligned} \quad (3.30)$$

and

$$\begin{aligned} K_{3sc}(q^2) &= +\frac{\alpha}{\sqrt{2}} \text{Im} \left\{ A_{\perp 1}^R A_{\perp 0}^{*R} - A_{\parallel 1}^R A_{\parallel 0}^{*R} + (R \leftrightarrow L) \right\}, \\ K_{3s}(q^2) &= +\frac{\alpha}{\sqrt{2}} \text{Im} \left\{ A_{\perp 1}^R A_{\parallel 0}^{*R} - A_{\parallel 1}^R A_{\perp 0}^{*R} - (R \leftrightarrow L) \right\}, \end{aligned} \quad (3.31)$$

and

$$\begin{aligned} K_{4sc}(q^2) &= +\frac{\alpha}{\sqrt{2}} \text{Re} \left\{ A_{\perp 1}^R A_{\parallel 0}^{*R} - A_{\parallel 1}^R A_{\perp 0}^{*R} + (R \leftrightarrow L) \right\}, \\ K_{4s}(q^2) &= +\frac{\alpha}{\sqrt{2}} \text{Re} \left\{ A_{\perp 1}^R A_{\perp 0}^{*R} - A_{\parallel 1}^R A_{\parallel 0}^{*R} - (R \leftrightarrow L) \right\}. \end{aligned} \quad (3.32)$$

The angular observables contain all the relevant information about the short- and long-distance dynamics in the SM or its extension by chirality-flipped operators in the effective Hamiltonian.

4 Phenomenological Applications

4.1 Simple Observables

For the experimental analyses one can construct weighted angular integrals of the differential decay width,

$$X(q^2) \equiv \int \frac{d^4\Gamma}{dq^2 d\cos\theta_\ell d\cos\theta_\Lambda d\phi} \omega_X(q^2, \cos\theta_\ell, \cos\theta_\Lambda, \phi) d\cos\theta_\ell d\cos\theta_\Lambda d\phi, \quad (4.1)$$

to obtain different decay distributions in the dilepton invariant mass q^2 as linear combinations of angular observables (or ratios thereof).

- (a) The simplest of these distributions is just the differential decay width in q^2 ,

$$\frac{d\Gamma}{dq^2} = 2K_{1ss} + K_{1cc}, \quad (4.2)$$

which corresponds to $\omega_X \equiv 1$.

- (b) The fraction of transverse or longitudinal polarization of the dilepton system is obtained as

$$F_1 = \frac{2K_{1cc}}{2K_{1ss} + K_{1cc}}, \quad F_0 = 1 - F_1 = \frac{2K_{1ss} - K_{1cc}}{2K_{1ss} + K_{1cc}}. \quad (4.3)$$

This is achieved by the weight functions

$$\omega_{F_1} = \frac{5\cos^2\theta_\ell - 1}{d\Gamma/dq^2}, \quad \omega_{F_0} = \frac{2 - 5\cos^2\theta_\ell}{d\Gamma/dq^2}. \quad (4.4)$$

- (c) The well-known forward-backward asymmetry with respect to the leptonic scattering angle, normalized to the differential rate, is defined as

$$A_{\text{FB}}^\ell = \frac{3}{2} \frac{K_{1c}}{2K_{1ss} + K_{1cc}}, \quad \omega_{A_{\text{FB}}^\ell} = \frac{\text{sgn}[\cos\theta_\ell]}{d\Gamma/dq^2}. \quad (4.5)$$

(d) The analogous asymmetry for the bayonic scattering angle reads

$$A_{\text{FB}}^{\Lambda} = \frac{1}{2} \frac{2K_{2ss} + K_{2cc}}{2K_{1ss} + K_{1cc}}, \quad \omega_{A_{\text{FB}}^{\Lambda}} = \frac{\text{sgn}[\cos \theta_{\Lambda}]}{d\Gamma/dq^2}. \quad (4.6)$$

(e) Finally, one can also study a combined forward-backward asymmetry via

$$A_{\text{FB}}^{\ell\Lambda} = \frac{3}{4} \frac{K_{2c}}{2K_{1ss} + K_{1cc}}, \quad \omega_{A_{\text{FB}}^{\ell\Lambda}} = \frac{\text{sgn}[\cos \theta_{\ell} \cos \theta_{\Lambda}]}{d\Gamma/dq^2}. \quad (4.7)$$

4.2 Exploiting Form-Factor Symmetries at Low Recoil

In the limit of low hadronic recoil to the $(N\pi)$ system (i.e. large invariant lepton mass $q^2 = \mathcal{O}(m_b^2) \gg \Lambda_{\text{QCD}}^2$), the number of independent form factors reduces as a consequence of the HQET spin symmetry [24]. In our notation the form-factor relation with the two leading Isgur-Wise functions ξ_1 and ξ_2 read (cf. [13])

$$\begin{aligned} \xi_1 - \xi_2 &= f_{\perp}^V = f_0^V = f_{\perp}^T = f_0^T, \\ \xi_1 + \xi_2 &= f_{\perp}^A = f_0^A = f_{\perp}^{T5} = f_0^{T5}. \end{aligned} \quad (4.8)$$

In phenomenological analyses, one can make use of these relations in the following way:

- At the moment, lattice-QCD estimates for the $\Lambda_b \rightarrow \Lambda$ form factors exist in the HQET limit [12]. These results, together with their respective uncertainties, can be implemented as a theoretical prior distribution for a Bayesian analysis of the experimental data (within the OPE/factorization approximation).
- Measuring suitably defined combinations of angular observables (see below), one can obtain experimental information about the size of corrections to the form-factor relations (4.8), in a similar way as has been proposed for the well-studied $B \rightarrow K^*(K\pi)\mu^+\mu^-$ decay [21, 23]. This will result in *independent* posterior distributions for the individual form factors, as found in [36–39].
- For the time being, priors for the individual form factors can be generated by estimates of Gaussian distributions for the subleading form factor contributions, which are defined in appendix A. In the long run, we expect lattice data for all individual form factors and their ratios.

In the following discussion, we will pursue a simplified approach that keeps the four contributing vector and axialvector form factors as independent hadronic quantities, and relates the four contributing tensor form factors via (4.8), including perturbative corrections at 1-loop (so called “improved Isgur-Wise relations, see appendix A). In this approximation each transversity amplitude is proportional to a single form factor and can be written as

$$A_{\perp 1}^{L(R)} \simeq -2N C_+^{L(R)} \sqrt{s_-} f_{\perp}^V(q^2), \quad A_{\parallel 1}^{L(R)} \simeq +2N C_-^{L(R)} \sqrt{s_+} f_{\perp}^A(q^2), \quad (4.9)$$

and

$$\begin{aligned} A_{\perp 0}^{L(R)} &\simeq +\sqrt{2} N C_+^{L(R)} \frac{m_{\Lambda_b} + m_{\Lambda}}{\sqrt{q^2}} \sqrt{s_-} f_0^V(q^2), \\ A_{\parallel 0}^{L(R)} &\simeq -\sqrt{2} N C_-^{L(R)} \frac{m_{\Lambda_b} - m_{\Lambda}}{\sqrt{q^2}} \sqrt{s_+} f_0^A(q^2), \end{aligned} \quad (4.10)$$

where we neglect $1/m_b$ corrections. The combinations of Wilson coefficients that appear in this way are given by

$$C_+^{R(L)} = \left((\mathcal{C}_9 + \mathcal{C}_{9'}) + \frac{2\kappa m_b m_{\Lambda_b}}{q^2} (\mathcal{C}_7 + \mathcal{C}_{7'}) \pm (\mathcal{C}_{10} + \mathcal{C}_{10'}) \right), \quad (4.11)$$

$$C_-^{R(L)} = \left((\mathcal{C}_9 - \mathcal{C}_{9'}) + \frac{2\kappa m_b m_{\Lambda_b}}{q^2} (\mathcal{C}_7 - \mathcal{C}_{7'}) \pm (\mathcal{C}_{10} - \mathcal{C}_{10'}) \right). \quad (4.12)$$

Here the parameter $\kappa = \kappa(\mu)$ contains the radiative QCD corrections to the form factor relations such that together with the product of Wilson coefficients and the b -quark mass the above expressions for the transversity amplitudes are renormalization-scale independent (in a given order of perturbation theory).

The simplification for the transversity amplitudes directly translates to the angular observables. It turns out that these are sensitive to the following combinations of short-distance parameters,

$$\begin{aligned} \rho_1^\pm &= \frac{1}{2} (|\mathcal{C}_\pm^R|^2 + |\mathcal{C}_\pm^L|^2) = |\mathcal{C}_{79} \pm \mathcal{C}_{7'9'}|^2 + |\mathcal{C}_{10} \pm \mathcal{C}_{10'}|^2, \\ \rho_2 &= \frac{1}{4} (\mathcal{C}_+^R \mathcal{C}_-^{R*} - \mathcal{C}_-^L \mathcal{C}_+^{L*}) \\ &= \text{Re} \{ \mathcal{C}_{79} \mathcal{C}_{10}^* - \mathcal{C}_{7'9'} \mathcal{C}_{10'}^* \} - i \text{Im} \{ \mathcal{C}_{79} \mathcal{C}_{7'9'}^* + \mathcal{C}_{10} \mathcal{C}_{10'}^* \}, \end{aligned} \quad (4.13)$$

that also appear in the angular observables for $B \rightarrow K^*(\rightarrow K\pi)\ell^+\ell^-$ decays [21, 23], and two new bilinears of Wilson coefficients

$$\rho_3^\pm = \frac{1}{2} (|\mathcal{C}_\pm^R|^2 - |\mathcal{C}_\pm^L|^2) = 2 \text{Re} \{ (\mathcal{C}_{79} \pm \mathcal{C}_{7'9'}) (\mathcal{C}_{10} \pm \mathcal{C}_{10'})^* \} \quad (4.14)$$

$$\begin{aligned} \rho_4 &= \frac{1}{4} (\mathcal{C}_+^R \mathcal{C}_-^{R*} + \mathcal{C}_-^L \mathcal{C}_+^{L*}) \\ &= (|\mathcal{C}_{79}|^2 - |\mathcal{C}_{7'9'}|^2 + |\mathcal{C}_{10}|^2 - |\mathcal{C}_{10'}|^2) - i \text{Im} \{ \mathcal{C}_{79} \mathcal{C}_{10'}^* - \mathcal{C}_{7'9'} \mathcal{C}_{10}^* \}, \end{aligned} \quad (4.15)$$

which contribute as a consequence of parity violation in the secondary weak decay.⁴ Here we abbreviate

$$\mathcal{C}_{79} \equiv \mathcal{C}_9^{\text{eff}} + \frac{2\kappa m_b m_{\Lambda_b}}{q^2} \mathcal{C}_7^{\text{eff}}, \quad \mathcal{C}_{7'9'} \equiv \mathcal{C}_{9'} + \frac{2\kappa m_b m_{\Lambda_b}}{q^2} \mathcal{C}_{7'}. \quad (4.16)$$

We observe that in this approximation $K_{3sc} = 0$ even in the presence of chirally-flipped operators.

⁴The combinations ρ_3^- and ρ_4 also emerge for the non-resonant $B \rightarrow K\pi\ell^+\ell^-$ decays as recently found in [40].

For the simple observables introduced in the previous subsection we then obtain

$$\frac{d\Gamma}{dq^2} = 4 |N|^2 \left\{ \rho_1^+ s_- \left[2 |f_\perp^V|^2 + \frac{(m_{\Lambda_b} + m_\Lambda)^2}{q^2} |f_0^V|^2 \right] + \rho_1^- s_+ \left[2 |f_\perp^A|^2 + \frac{(m_{\Lambda_b} - m_\Lambda)^2}{q^2} |f_0^A|^2 \right] \right\}, \quad (4.17)$$

and

$$F_0 = 4 |N|^2 \left\{ \rho_1^+ s_- \frac{(m_{\Lambda_b} + m_\Lambda)^2}{q^2} |f_0^V|^2 + \rho_1^- s_+ \frac{(m_{\Lambda_b} - m_\Lambda)^2}{q^2} |f_0^A|^2 \right\} \left(\frac{d\Gamma}{dq^2} \right)^{-1}, \quad (4.18)$$

and

$$\begin{aligned} \frac{d\Gamma}{dq^2} A_{\text{FB}}^\ell &= 24 |N|^2 \text{Re} \{ \rho_2 \} \sqrt{s_+ s_-} f_\perp^V f_\perp^A, \\ \frac{d\Gamma}{dq^2} A_{\text{FB}}^\Lambda &= -8 |N|^2 \alpha \text{Re} \{ \rho_4 \} \sqrt{s_+ s_-} \left\{ 2 f_\perp^V f_\perp^A + \frac{m_{\Lambda_b}^2 - m_\Lambda^2}{q^2} f_0^V f_0^A \right\}, \\ \frac{d\Gamma}{dq^2} A_{\text{FB}}^{\ell\Lambda} &= -3 |N|^2 \alpha \{ \rho_3^+ s_- |f_\perp^V|^2 + \rho_3^- s_+ |f_\perp^A|^2 \}. \end{aligned} \quad (4.19)$$

We will present numerical estimates for these observables in the SM (integrated over q^2 in the low-recoil region) in section 4.4.

Future experimental data will also allow to simultaneously test the short-distance structure of the SM against NP, and to extract information on form-factor ratios. In the presence of both SM-like and chirality-flipped operators, we find one ratio of angular observables where the form factors cancel *in the given approximation*,

$$X_1 \equiv \frac{K_{1c}}{K_{2cc}} = -\frac{\text{Re} \{ \rho_2 \}}{\alpha \text{Re} \{ \rho_4 \}}, \quad (4.20)$$

and two ratios of angular observables which only depend on form factors,

$$\begin{aligned} \frac{2 K_{2ss}}{K_{2cc}} &= 1 + \frac{m_{\Lambda_b}^2 - m_\Lambda^2}{q^2} \frac{f_0^V f_0^A}{f_\perp^V f_\perp^A}, \\ \frac{2 K_{4sc}}{K_{2cc}} &= \frac{m_{\Lambda_b} + m_\Lambda}{\sqrt{q^2}} \frac{f_0^V}{f_\perp^V} - \frac{m_{\Lambda_b} - m_\Lambda}{\sqrt{q^2}} \frac{f_0^A}{f_\perp^A}. \end{aligned} \quad (4.21)$$

We also find ratios that are only functions of the Wilson coefficients and a single ratio of form factors, f_\perp^V/f_\perp^A ,

$$\begin{aligned} \frac{4 K_{1cc}}{K_{1c}} &= \sqrt{\frac{s_-}{s_+}} \frac{\rho_1^+}{\text{Re} \{ \rho_2 \}} \frac{f_\perp^V}{f_\perp^A} + \sqrt{\frac{s_+}{s_-}} \frac{\rho_1^-}{\text{Re} \{ \rho_2 \}} \frac{f_\perp^A}{f_\perp^V}, \\ \frac{4 K_{2c}}{K_{2cc}} &= \sqrt{\frac{s_-}{s_+}} \frac{\rho_3^+}{\text{Re} \{ \rho_4 \}} \frac{f_\perp^V}{f_\perp^A} + \sqrt{\frac{s_+}{s_-}} \frac{\rho_3^-}{\text{Re} \{ \rho_4 \}} \frac{f_\perp^A}{f_\perp^V}. \end{aligned} \quad (4.22)$$

If, on the other hand, we assume the absence of chirality-flipped operators (including $\mathcal{C}_{7\prime} \rightarrow 0$ in the SM), we obtain

$$\rho_3^\pm \rightarrow 2\rho_2 = 2\operatorname{Re}\{\mathcal{C}_{79}\mathcal{C}_{10}^*\} \quad \text{and} \quad \rho_4 \rightarrow \frac{1}{2}\rho_1 = \frac{1}{2}(|\mathcal{C}_{79}|^2 + |\mathcal{C}_{10}|^2). \quad (4.23)$$

This further implies $K_{3s} \rightarrow 0$, and we also find one more ratio of observables which is free of form factors,

$$X_1 \rightarrow -\frac{2\rho_2}{\alpha\rho_1}, \quad X_2 \equiv \frac{K_{1cc}}{K_{2c}} = -\frac{2\alpha\rho_2}{\rho_1}. \quad (4.24)$$

The additional short-distance free observables in the SM operator basis are given by

$$\begin{aligned} \frac{2K_{1ss} - K_{1cc}}{K_{1cc}} &= \frac{s_- (m_{\Lambda_b} + m_\Lambda)^2 |f_0^V|^2 + s_+ (m_{\Lambda_b} - m_\Lambda)^2 |f_0^A|^2}{q^2 s_- |f_\perp^V|^2 + q^2 s_+ |f_\perp^A|^2}, \\ \frac{2K_{1ss} - K_{1cc}}{2K_{2ss} - K_{2cc}} &= -\frac{1}{2\alpha} \left(\frac{f_0^V}{f_0^A} \sqrt{\frac{s_-}{s_+}} \frac{m_{\Lambda_b} + m_\Lambda}{m_{\Lambda_b} - m_\Lambda} + \frac{f_0^A}{f_0^V} \sqrt{\frac{s_+}{s_-}} \frac{m_{\Lambda_b} - m_\Lambda}{m_{\Lambda_b} + m_\Lambda} \right), \\ \alpha^2 \frac{K_{1cc}}{K_{2cc}} = \frac{K_{2c}}{K_{1c}} &= -\frac{\alpha}{2} \left(\sqrt{\frac{s_-}{s_+}} \frac{f_\perp^V}{f_\perp^A} + \sqrt{\frac{s_+}{s_-}} \frac{f_\perp^A}{f_\perp^V} \right). \end{aligned} \quad (4.25)$$

4.3 Simplifications at Large Recoil

The number of independent form factors reduces further in the limit of large recoil energy [41, 42] where the leading contributions⁵ can be identified using soft-collinear effective theory (SCET [43, 44]). In our notation this simply implies the equality of all helicity form factors,

$$f_\perp^V = f_0^V = f_\perp^T = f_0^T = f_\perp^A = f_0^A = f_\perp^{T5} = f_0^{T5}. \quad (4.26)$$

Including α_s corrections to the soft form factors, the modification of the form-factor relations (4.26) can be described by a vertex factor, and a single q^2 -dependent function $\Delta\xi_\Lambda$ that emerges from spectator scattering, see appendix C of [13]. The values of ξ_Λ and $\Delta\xi_\Lambda$ have been estimated from sum rules with Λ_b distribution amplitudes in [13]. Due to the complexity of the baryonic transition and – compared to the mesonic case – the poor theoretical knowledge on the baryonic wave functions, these estimates have a large uncertainty. With sufficient experimental information, however, one can again try to constrain the form-factor values from the data itself.

To this end, we first recall that the function $\Delta\xi_\Lambda$ drops out in the following sums,

$$\begin{aligned} \frac{f_0^V + f_0^A}{2} \equiv \xi_\Lambda &\Rightarrow \frac{f_\perp^V + f_\perp^A}{2} \simeq \left(1 + \frac{\alpha_s C_F}{4\pi} L \right) \xi_\Lambda, \\ \frac{f_0^T + f_0^{T5}}{2} &\simeq \left(1 + \frac{\alpha_s C_F}{4\pi} \left(\ln \frac{m_b^2}{\mu^2} - 2 + 2L \right) \right) \xi_\Lambda, \\ \frac{f_\perp^T + f_\perp^{T5}}{2} &\simeq \left(1 + \frac{\alpha_s C_F}{4\pi} \left(\ln \frac{m_b^2}{\mu^2} - 2 \right) \right) \xi_\Lambda. \end{aligned} \quad (4.27)$$

⁵More precisely, one has to distinguish soft overlap contributions [13, 25] and hard spectator interactions [11]. In contrast to the analogous B -meson transitions, the former are suppressed by one power of the b -quark mass compared to the latter. On the other hand, the hard spectator term now only starts at second order in the strong coupling α_s and therefore numerically appears to be a sub-dominant effect. In any case, both contributions fulfill the form-factor symmetry relations to first approximation.

where $L = \frac{q^2 - m_b^2}{q^2} \ln \left(1 - \frac{q^2}{m_b^2} \right)$, and the μ -dependence of the tensor form factors related to the anomalous dimension of the tensor operators is explicit. The corresponding *differences* between form factors will be proportional to $\Delta\xi_\Lambda$. We remind the reader that in the large-recoil region we also expect sizeable corrections from non-factorizable (i.e. not form-factor like) contributions, which formally enter at the same order as $\Delta\xi_\Lambda$. These have not been calculated or estimated at present, but would be required for a consistent extraction of $\Delta\xi_\Lambda$. The phenomenological strategy would then be the following.

- Take (4.27) as a theoretical constraint on the form factors.
- Use $f_0^V - f_0^A \rightarrow f_\perp^V - f_\perp^A \rightarrow f_0^T - f_0^{T5} \rightarrow f_\perp^T - f_\perp^{T5} \rightarrow 0$ as the central value for a theory prior on the form-factor differences with a conservative estimate for the theory uncertainty (say, of the order 20-30%, independently for each individual form factor difference).
- Based on comparison with upcoming experimental data, posterior predictive distributions for the form-factor differences $f_0^V - f_0^A$ and $f_\perp^V - f_\perp^A$ can be obtained. (Further differences could be constrained if data permits). These would indicate the size of corrections to the large-recoil symmetry relations. Using an explicit ansatz for both the factorizable and non-factorizable spectator effects, the size of these effects could be estimated.

As a first step, we may ignore the spectator effects altogether. Including the known factorizing contributions from the relevant hadronic operators in $b \rightarrow s\ell^+\ell^-$ processes [45], the transversity amplitudes can then be written as

$$\begin{aligned}
A_{\perp 1}^{L(R)} &= -2N \left[C_{9,10,+}^{L(R)} + \frac{2m_b m_{\Lambda_b}}{q^2} \tau_{1,+} \right] f_\perp^V \sqrt{s_-}, \\
A_{\parallel 1}^{L(R)} &= +2N \left[C_{9,10,-}^{L(R)} + \frac{2m_b m_{\Lambda_b}}{q^2} \tau_{1,-} \right] f_\perp^A \sqrt{s_+}, \\
A_{\perp 0}^{L(R)} &= +\sqrt{2}N \left[C_{9,10,+}^{L(R)} + \frac{2m_b}{m_{\Lambda_b}} \tau_{0,+} \right] f_0^V \sqrt{s_-}, \\
A_{\parallel 0}^{L(R)} &= -\sqrt{2}N \left[C_{9,10,-}^{L(R)} + \frac{2m_b}{m_{\Lambda_b}} \tau_{0,-} \right] f_0^A \sqrt{s_+},
\end{aligned} \tag{4.28}$$

where the quantities $\tau_{i,\pm}$ can be expressed in terms of Wilson coefficients \mathcal{C}_i , form-factor ratios R_i and perturbative functions $F_i^{(7,9)}$,

$$\begin{aligned}
\tau_{1,\pm} &= \frac{m_{\Lambda_b} \pm m_\Lambda}{m_{\Lambda_b}} \left(\mathcal{C}_7^{\text{eff}} \pm \mathcal{C}_{7'} - \frac{\alpha_s}{4\pi} \sum_{i=1,2,8} \mathcal{C}_i F_i^{(7)}(q^2, m_b, m_c) \right) R_1 \\
&\quad + \frac{q^2}{2m_b m_{\Lambda_b}} \left(Y_9(q^2) - \frac{\alpha_s}{4\pi} \sum_{i=1,2,8} \mathcal{C}_i F_i^{(9)}(q^2, m_b, m_c) \right), \\
\tau_{0,\pm} &= \frac{m_{\Lambda_b}}{m_{\Lambda_b} \pm m_\Lambda} \left(\mathcal{C}_7^{\text{eff}} \pm \mathcal{C}_{7'} - \frac{\alpha_s}{4\pi} \sum_{i=1,2,8} \mathcal{C}_i F_i^{(7)}(q^2, m_b, m_c) \right) R_0
\end{aligned}$$

$$+ \frac{m_{\Lambda_b}}{2m_b} \left(Y_9(q^2) - \frac{\alpha_s}{4\pi} \sum_{i=1,2,8} C_i F_i^{(9)}(q^2, m_b, m_c) \right). \quad (4.29)$$

and the function $Y_9(q^2)$ captures the one-loop virtual quark-loop contribution which can be absorbed into $C_9 \rightarrow C_9^{\text{eff}}(q^2)$. The form-factor ratios occurring in this limit are simply given by

$$\begin{aligned} R_1 &= \frac{f_{\perp}^T}{f_{\perp}^V} = \frac{f_{\perp}^{T5}}{f_{\perp}^A} = 1 + \frac{\alpha_s C_F}{4\pi} \left(\ln \left(\frac{m_b^2}{\mu^2} - 2 - L \right) \right), \\ R_0 &= \frac{f_0^T}{f_0^V} = \frac{f_0^{T5}}{f_0^A} = 1 + \frac{\alpha_s C_F}{4\pi} \left(\ln \left(\frac{m_b^2}{\mu^2} - 2 + 2L \right) \right), \end{aligned} \quad (4.30)$$

The three observable forward-backward asymmetries, $A_{\text{FB}}^{\ell, \Lambda, \ell \Lambda}(q^2)$, develop a characteristic q^2 -behaviour (see numerical discussion below). In particular, we find that within the SM $A_{\text{FB}}^{\ell}(q^2)$ and $A_{\text{FB}}^{\ell \Lambda}(q^2)$ cross zero, where to first approximations the roots $q_{0,\ell}^2$ and $q_{0,\ell \Lambda}^2$ are the same,

$$q_{0,\ell}^2 \simeq q_{0,\ell \Lambda}^2 \simeq -2 m_b m_{\Lambda_b} \frac{C_7}{C_9}. \quad (4.31)$$

This expression is well known from other exclusive and the inclusive $b \rightarrow s \ell^+ \ell^-$ decays. On the other hand, $A_{\text{FB}}^{\Lambda}(q^2)$ does not cross zero in the SM.

4.4 Numerical Analysis

In order to translate our theoretical results into numerical predictions, we are going to determine predictive probability distributions for the $\Lambda_b \rightarrow \Lambda(\rightarrow N\pi)\ell^+\ell^-$ observables. All central values and uncertainty ranges that we quote are based on these distributions. In the course of our work, we extend the EOS flavor program [46] through implementation of the relevant decay observables at both large and low hadronic recoil.

4.4.1 Transition Form Factors

Within our simplified factorization approach, the essential hadronic input functions are the $\Lambda_b \rightarrow \Lambda$ transition form factors. For the numerical analysis we need probability distributions for the individual helicity form-factor values at different values of q^2 . To this end we take into account the available lattice data in the heavy-quark limit and an estimate of the soft form factor from a sum rule in the large-recoil limit, which are combined using the parametrization eq. (B.2). Corrections to the heavy-quark limit are allowed for as well.

The specific steps of our analysis aim toward a Bayesian analysis once the knowledge of the transition form factors improves. These steps are presented in detail in appendix C.

Our setup includes eight form factor parameters \vec{x} , see eq. (C.6). The main result of the fits is the *posterior* $P(\vec{x}|\text{Estimates})$, which is defined in eq. (C.13). The posterior is central to the computation of the numerical results that follow.

4.4.2 Results

Theory uncertainties in the computation of the observables arise, beyond the transition form factors, also from variations of CKM matrix elements, the $\Lambda \rightarrow N\pi$ coupling α , and the masses of the charm and bottom quark; see table 1 for a summary.

For the CKM matrix elements, we use uncorrelated Gaussian distributions for our analysis. Their parameters follow from the marginalised posterior distributions as obtained by the UFit collaboration in their ‘‘Tree Level Fit’’ analysis [47]. For α and the quark masses, we use world averages as provided by the Particle Data Group [48]. Further input parameters, such as the hadron masses and lifetimes, are fixed to the central values of their respective world averages [48]. For the Λ_b lifetime, we use the more recent world average by the Heavy Flavor Averaging Group [49],

$$\tau_{\Lambda_b}^{\text{HFAG}} = 1.451 \pm 0.013 \text{ ps}, \quad (4.32)$$

which includes the two recent measurements by the LHCb collaboration [50, 51].

The observables of interest in our analysis are the branching ratio \mathcal{B} , the three forward-backward asymmetries A_{FB}^ℓ , A_{FB}^Λ and $A_{\text{FB}}^{\ell\Lambda}$, and the fraction of longitudinal lepton pairs F_0 . For the numerical evaluation, we first calculate q^2 -integrated angular observables $K_{n\lambda}$. All observables of interest are then computed from these pre-integrated angular observables, which we denote as $\langle O \rangle$ for any observable $O(q^2)$. Our nominal choice of the integration region is $15 \text{ GeV}^2 \leq q^2 \leq (m_{\Lambda_b} - m_\Lambda)^2$, in order to minimize the uncertainties from quark-hadron duality violation (see the discussion for the mesonic counterpart in [52]).⁶

We obtain numerical estimates for the observables \vec{O} through uncertainty propagation. For this, we compute $8 \cdot 10^5$ variates of the predictive distribution $P(\vec{O})$,

$$P(\vec{O}) = \iint d\vec{x} d\vec{v} \delta(\vec{O} - \vec{O}(\vec{x}, \vec{v})) P(\vec{x}|\text{Estimates}) P_0(\vec{v}). \quad (4.33)$$

Here, $P_0(\vec{v})$ is the prior of our nuisance parameters \vec{v} . The nuisance parameters encompass all parameters that are listed in table 1, as well as the parameters $r_\lambda^{\Gamma, \tilde{\Gamma}}$ that are specified in appendix C.

For the nominal integration range we obtain the modes of the marginalized distributions and their minimal 68% probability intervals as

$$\begin{aligned} \langle \mathcal{B} \rangle &= (4.5 \pm 1.2) \cdot 10^{-7}, \\ \langle A_{\text{FB}}^\ell \rangle &= -0.29 \pm 0.05, \\ \langle A_{\text{FB}}^\Lambda \rangle &= -0.26 \pm 0.03, \\ \langle A_{\text{FB}}^{\ell\Lambda} \rangle &= +0.13_{-0.03}^{+0.02}, \\ \langle F_0 \rangle &= +0.4 \pm 0.1. \end{aligned} \quad (4.34)$$

⁶Note that in view of the present experimental situation [53] the effects from quark-hadron duality violation can still be sizable, even after averaging over the entire low-recoil region. A local description of the spectrum, similar to the mesonic case as discussed in [54–56], is beyond the scope of this work.

In addition, we compare our result for the somewhat larger q^2 bin $14.18 \text{ GeV}^2 \leq q^2 \leq (m_{\Lambda_b} - m_\Lambda)^2$ at 68% probability,

$$\langle \mathcal{B} \rangle = (5.3_{-1.3}^{+1.5}) \cdot 10^{-7}, \quad (4.35)$$

with our naive combination of the the experimental measurements in two low-recoil bins [5]⁷,

$$\langle \mathcal{B} \rangle^{\text{LHCb}} = (6.2 \pm 2.1) \cdot 10^{-7}. \quad (4.36)$$

We find good agreement between our prediction and the measurement, which is not surprising given the substantial uncertainties that affect both the prediction of the branching ratio and the experimental measurement of the same.

In light of the present tension between the recent LHCb measurement with some of the SM predictions [57] – see also [58] for more compatible predictions – we further investigate the BSM reach of the angular observables. For this, we carry out a numerical study of the observables $X_{1,2}$ as previously defined in eq. (4.20) and eq. (4.24). Similar to observables in the decay $\bar{B} \rightarrow \bar{K}^*(\rightarrow \bar{K}\pi)\ell^+\ell^-$, the observables $X_{1,2}$ are constructed so that at small q^2 the leading form factor ξ_Λ cancels. In addition, they are sensitive toward BSM effects, specifically right-handed currents. At large q^2 , X_1 remains insensitive to the hadronic form factors, while X_2 develops a small form factor dependence in BSM models with right-handed currents. For illustration, we produce SM estimates that are compared to estimates within two benchmark scenarios BM1 and BM2. We define the latter scenarios as

$$\mathcal{C}_9^{\text{BM1}} = \mathcal{C}_9^{\text{SM}} - 1, \quad \mathcal{C}_{9'}^{\text{BM1}} = 1, \quad (4.37)$$

and

$$\begin{aligned} \mathcal{C}_7^{\text{BM2}} &= +0.15, & \mathcal{C}_9^{\text{BM2}} &= 0.0, & \mathcal{C}_{10}^{\text{BM2}} &= -1.0, \\ \mathcal{C}_{7'}^{\text{BM2}} &= +0.40, & \mathcal{C}_{9'}^{\text{BM2}} &= -4.0, & \mathcal{C}_{10'}^{\text{BM2}} &= -4.5, \end{aligned} \quad (4.38)$$

while the rest of the Wilson coefficients remain as in the SM, respectively. Our motivation for these scenarios stems from a comprehensive analysis of available $b \rightarrow s$ -FCNC decays [39]; see also [59, 60] for further works. Specifically, scenario BM1 corresponds to the best-fit point in a constrained fit of only $\mathcal{C}_{9,9'}$, as can be seen in figure 4 of [39]. Scenario BM2 corresponds to solution D' in a fit to the SM and chirality-flipped Wilson coefficients, as can be seen in figure 3 of [39]. Both scenarios can explain the present tension at 68% probability, since they follow paths in the parameter space of Wilson coefficients that – for instance – leave the bilinears ρ_1^\pm and ρ_2 constant. However, both scenarios yield different results for the bilinears ρ_3^\pm and ρ_4 , which are presently unconstrained. We thus expect to be able to discriminate them based on sufficiently precise measurements of $\Lambda_b \rightarrow \Lambda(\rightarrow N\pi)\ell^+\ell^-$ observables.

For the low recoil bin $15 \text{ GeV}^2 \leq q^2 \leq (m_{\Lambda_b} - m_\Lambda)^2$ we obtain

$$\langle X_1 \rangle^{\text{SM}} = +1.54_{-0.04}^{+0.03}, \quad \langle X_1 \rangle^{\text{BM1}} = +1.55_{-0.04}^{+0.05}, \quad \langle X_1 \rangle^{\text{BM2}} = -1.67_{-0.05}^{+0.05}, \quad (4.39)$$

$$\langle X_2 \rangle^{\text{SM}} = +0.63_{-0.01}^{+0.01}, \quad \langle X_2 \rangle^{\text{BM1}} = +0.60_{-0.03}^{+0.02}, \quad \langle X_2 \rangle^{\text{BM2}} = -0.60_{-0.02}^{+0.02}. \quad (4.40)$$

⁷We neglect small correlation effects when combining the experimental measurements of the two low recoil bins.

parameter	value and 68% interval	unit	source
λ	0.2253 ± 0.0006		[47]
A	0.806 ± 0.020		[47]
$\bar{\rho}$	0.132 ± 0.049		[47]
$\bar{\eta}$	0.369 ± 0.050		[47]
α	0.642 ± 0.013		[48]
$\overline{m_c}(m_c)$	1.275 ± 0.025	GeV	[48]
$\overline{m_b}(m_b)$	4.18 ± 0.03	GeV	[48]

Table 1. Summary of the prior distributions for the nuisance parameters $\vec{\nu}$ (except form factor ratios) that enter the observables in addition to the form factor parameters \vec{x} .

For the commonly used large recoil bin $1 \text{ GeV}^2 \leq q^2 \leq 6 \text{ GeV}^2$ we find

$$\langle X_1 \rangle^{\text{SM}} = +0.08_{-0.09}^{+0.12}, \quad \langle X_1 \rangle^{\text{BM1}} = -0.49_{-0.08}^{+0.07}, \quad \langle X_1 \rangle^{\text{BM2}} = +0.35_{-0.15}^{+0.10}, \quad (4.41)$$

$$\langle X_2 \rangle^{\text{SM}} = +0.17_{-0.17}^{+0.04}, \quad \langle X_2 \rangle^{\text{BM1}} = -0.22_{-0.03}^{+0.03}, \quad \langle X_2 \rangle^{\text{BM2}} = +0.33_{-0.31}^{+0.09}. \quad (4.42)$$

In both cases, the estimation of uncertainties is the same as for the simple observables above. However, we emphasize that the uncertainty estimate for the large recoil region is not very rigorous because numerically important contributions from hard spectator interactions are not yet known.

Our numerical estimates clearly show that the observables $X_{1,2}$ are capable to distinguish between the benchmark models BM1, BM2 and the SM as measurements both at large and at low hadronic recoil are taken into account. In particular, a distinction between the SM and BM1 can be made using precise measurements of $X_{1,2}$ at small q^2 . Similarly, the SM and BM2 can be distinguished using large- q^2 measurements.

5 Summary and Outlook

In the present article we have investigated the phenomenological potential of the rare decay $\Lambda_b \rightarrow \Lambda \ell^+ \ell^-$ with a subsequent, self-analyzing $\Lambda \rightarrow N \pi$ transition. From the kinematics of the primary and secondary decay we have worked out the fully differential decay width that follows from the Standard Model (SM) operator basis for radiative $b \rightarrow s$ transitions and its chirality-flipped counterpart which may be relevant for physics beyond the SM. Similar to the corresponding mesonic decay, $B \rightarrow (K^* \rightarrow K \pi) \ell^+ \ell^-$, the differential decay width can be expressed in terms of 10 angular observables. In the (naive) factorization approximation, these can be conveniently expressed in terms of short-distance Wilson coefficients and hadronic transition form factors in the helicity or transversity basis.

Exploiting the simplifications that arise in the heavy b -quark mass limit – notably the form-factor relations that arise in the framework of heavy-quark effective theory for low

recoil, or soft-collinear effective theory for large recoil – we have discussed the phenomenological consequences for some interesting observables: In the SM the fraction of transverse dilepton polarization, and various forward-backward asymmetries in the leptonic or baryonic variables show a characteristic dependence on the leptonic invariant mass q^2 which can be confronted with experimental data.

Numerical predictions for these observables have been obtained on the basis of a careful statistical analysis of the presently available estimates of hadronic input parameters and their (correlated) uncertainties. We have also identified a number of ratios of angular observables where either the short-distance Wilson coefficients or the long-distance form factors drop out to first approximation. In particular, as a consequence of the parity-violating nature of the secondary decay, we have found that the angular analysis of the $\Lambda_b \rightarrow \Lambda(\rightarrow N\pi)\ell^+\ell^-$ decay is sensitive to combinations of Wilson coefficients that cannot be directly tested in $B \rightarrow K^*(\rightarrow K\pi)\ell^+\ell^-$ decays. Future experimental information on these ratios can thus be used to complement the on-going search for new physics from rare radiative $b \rightarrow s$ transitions.

Compared to the mesonic counterpart decays, $B \rightarrow K^{(*)}\ell^+\ell^-$, both the theoretical and experimental situation is not yet competitive: Detailed experimental information, in particular for the large-recoil region, is still lacking at the moment; from the theoretical side, a systematic analysis of non-factorizable hadronic effects (i.e. not form-factor like) is still missing. Both issues are expected to be (at least partially) solved in the future, and the decay $\Lambda_b \rightarrow \Lambda(\rightarrow N\pi)\ell^+\ell^-$ can thus play an important role in the flavour-physics program at the Large Hadron Collider.

Acknowledgements

D.v.D would like to thank Patrick Jussel and Michal Kreps for discussions regarding the experimental analysis of $\Lambda_b \rightarrow \Lambda\ell^+\ell^-$ decays, and Imkong Sentitemsu Imsong and Thomas Mannel for discussions on $\Lambda_b \rightarrow \Lambda$ form factors. We would also like to thank the authors of [40] for sharing their results with us prior to publication.

We are grateful to Stefan Meinel for pointing out a typo in eq. (3.28). This work is supported in parts by the Bundesministerium für Bildung und Forschung (BMBF), and by the Deutsche Forschungsgemeinschaft (DFG) within Research Unit FOR 1873 (“Quark Flavour Physics and Effective Field Theories”).

A Corrections to HQET Form Factor Relations

In the low-recoil region, the $\Lambda_b \rightarrow \Lambda$ form factors are related by HQET spin symmetries in the heavy-quark limit. We follow the analysis in [61] and take into account sub-leading terms in α_s and $1/m_b$ appearing in the matching of QCD currents to HQET. For the vector and axial-vector currents this amounts to

$$\begin{aligned}\bar{s}\gamma^\mu b &= C_0^{(v)} \bar{s}\gamma^\mu h_v + C_1^{(v)} v^\mu \bar{s}h_v + \frac{1}{2m_b} \bar{s}\gamma^\mu i\not{D}_\perp h_v + \dots, \\ \bar{s}\gamma^\mu\gamma_5 b &= C_0^{(v)} \bar{s}\gamma^\mu\gamma_5 h_v - C_1^{(v)} v^\mu \bar{s}\gamma_5 h_v - \frac{1}{2m_b} \bar{s}\gamma^\mu i\not{D}_\perp\gamma_5 h_v + \dots,\end{aligned}\tag{A.1}$$

and for the tensor and pseudotensor currents one has

$$\bar{s}i\sigma^{\mu\nu}q_\nu(\gamma_5)b = C_0^{(t)}\bar{s}i\sigma^{\mu\nu}q_\nu(\gamma_5)h_v \pm \frac{1}{2m_b}\bar{s}\sigma^{\mu\nu}q_\nu i\mathcal{D}_\perp(\gamma_5)h_v + \dots \quad (\text{A.2})$$

Here the leading-power matching coefficients at NLO read

$$\begin{aligned} C_0^{(v)}(\mu) &= 1 - \frac{\alpha_s C_F}{4\pi} \left(3 \ln \left(\frac{\mu}{m_b} \right) + 4 \right) + \mathcal{O}(\alpha_s^2), \\ C_1^{(v)}(\mu) &= \frac{\alpha_s C_F}{2\pi} + \mathcal{O}(\alpha_s^2), \\ C_0^{(t)}(\mu) &= 1 - \frac{\alpha_s C_F}{4\pi} \left(5 \ln \left(\frac{\mu}{m_b} \right) + 4 \right) + \mathcal{O}(\alpha_s^2). \end{aligned} \quad (\text{A.3})$$

The hadronic matrix elements of these currents can then be parametrized in terms of leading and sub-leading Isgur-Wise functions, denoted as $\xi_n \equiv \xi_n(v \cdot k)$ and $\chi_m \equiv \chi_m(v \cdot k)$, respectively:

$$\begin{aligned} &\langle \Lambda(k, s_\Lambda) | \bar{s}\gamma^\mu(\gamma_5)b | \Lambda_b(p = m_{\Lambda_b}v, s_{\Lambda_b}) \rangle \\ &\simeq C_0^{(v)} \sum_{n=1,2} \xi_n \bar{u}_\Lambda(k, s_\Lambda) \Gamma_n \gamma^\mu(\gamma_5) u_{\Lambda_b}(v, s_{\Lambda_b}) \\ &\quad \pm C_1^{(v)} \sum_{n=1,2} \xi_n v^\mu \bar{u}_\Lambda(k, s_\Lambda) \Gamma_n(\gamma_5) u_{\Lambda_b}(v, s_{\Lambda_b}) \\ &\quad \pm \sum_m \frac{\chi_m}{2m_b} \bar{u}_\Lambda(k, s_\Lambda) \hat{\Gamma}_m \gamma^\mu(\gamma_5) \tilde{\Gamma}_m u_{\Lambda_b}(v, s_{\Lambda_b}) \end{aligned} \quad (\text{A.4})$$

and

$$\begin{aligned} &\langle \Lambda(k, s_\Lambda) | \bar{s}i\sigma^{\mu\nu}q_\nu(\gamma_5)b | \Lambda_b(p = m_{\Lambda_b}v, s_{\Lambda_b}) \rangle \\ &\simeq C_0^{(t)} \sum_{n=1,2} \xi_n \bar{u}_\Lambda(k, s_\Lambda) \Gamma_n i\sigma^{\mu\nu}q_\nu(\gamma_5) u_{\Lambda_b}(v, s_{\Lambda_b}) \\ &\quad \pm \sum_m \frac{\chi_m}{2m_b} \bar{u}_\Lambda(k, s_\Lambda) \hat{\Gamma}_m i\sigma^{\mu\nu}q_\nu(\gamma_5) \tilde{\Gamma}_m u_{\Lambda_b}(v, s_{\Lambda_b}). \end{aligned} \quad (\text{A.5})$$

Here, the independent Dirac structures are given by

$$\Gamma_1 = 1, \quad \Gamma_2 = \not{v}, \quad (\text{A.6})$$

for the leading-power terms, and

$$\begin{aligned} \hat{\Gamma}_1 &= m_\Lambda \gamma_\mu, & \tilde{\Gamma}_1 &= \gamma_\perp^\mu, \\ \hat{\Gamma}_2 &= k_\mu, & \tilde{\Gamma}_2 &= \gamma_\perp^\mu, \\ \hat{\Gamma}_3 &= m_\Lambda \gamma_\mu \gamma_5, & \tilde{\Gamma}_3 &= \gamma_\perp^\mu \gamma_5, \\ \hat{\Gamma}_4 &= k_\mu \gamma_5, & \tilde{\Gamma}_4 &= \gamma_\perp^\mu \gamma_5, \\ \hat{\Gamma}_5 &= \frac{i}{2} \gamma^\mu \gamma_5, & \tilde{\Gamma}_5 &= \gamma_\perp^\nu v^\alpha k^\beta \varepsilon_{\mu\nu\alpha\beta}, \\ \hat{\Gamma}_6 &= \frac{i}{2} \gamma^\mu, & \tilde{\Gamma}_6 &= \gamma_\perp^\nu \gamma_5 v^\alpha k^\beta \varepsilon_{\mu\nu\alpha\beta}, \end{aligned} \quad (\text{A.7})$$

J^P	0^-	0^+	1^-	1^+
mass [GeV ²]	5.367	unknown	5.415	5.829

Table 2. List of low-lying B_s resonances for the transition form factor $\Lambda_b \rightarrow \Lambda$ as taken from [48]

for the terms at subleading power. For the physical form factors this translates into

$$f_{\perp}^{V,A} = C_0^{(v)}(\xi_1 \mp \xi_2) - \frac{m_{\Lambda}(\chi_1 + \chi_3)}{2m_b} \mp \frac{s_{\pm}(\chi_2 + \chi_4)}{4m_b m_{\Lambda_b}} \quad (\text{A.8})$$

$$\begin{aligned} f_0^{V,A} = & \left(C_0^{(v)} + \frac{C_1^{(v)} s_{\pm}}{2m_{\Lambda_b}(m_{\Lambda_b} \pm m_{\Lambda})} \right) \xi_1 \mp \left(C_0^{(v)} - \frac{(2C_0^{(v)} + C_1^{(v)})s_{\pm}}{2m_{\Lambda_b}(m_{\Lambda_b} \pm m_{\Lambda})} \right) \xi_2 \\ & - \frac{m_{\Lambda}}{2m_b} \left(1 + \frac{s_{\pm}}{m_{\Lambda_b}(m_{\Lambda_b} \pm m_{\Lambda})} \right) (\chi_1 + \chi_3) \\ & \pm \frac{s_{\pm}}{4m_b m_{\Lambda_b}} \frac{m_{\Lambda_b} \mp m_{\Lambda}}{m_{\Lambda_b} \pm m_{\Lambda}} [(\chi_2 + \chi_4) \pm (\chi_5 + \chi_6)], \end{aligned} \quad (\text{A.9})$$

and

$$\begin{aligned} f_{\perp}^{T(5)} = & C_0^{(t)} \left((\xi_1 \mp \xi_2) \pm \frac{s_{\pm}}{m_{\Lambda_b}(m_{\Lambda_b} \pm m_{\Lambda})} \xi_2 \right) \\ & + \frac{m_{\Lambda}}{2m_b} \left(1 - \frac{s_{\pm}}{m_{\Lambda_b}(m_{\Lambda_b} \pm m_{\Lambda})} \right) (\chi_1 - \chi_3) \\ & \pm \frac{m_{\Lambda_b} \mp m_{\Lambda}}{m_{\Lambda_b} \pm m_{\Lambda}} \frac{s_{\pm}}{4m_b m_{\Lambda_b}} (\chi_2 - \chi_4), \end{aligned} \quad (\text{A.10})$$

$$f_0^{T(5)} = C_0^{(t)}(\xi_1 \mp \xi_2) + \frac{m_{\Lambda}}{2m_b}(\chi_1 - \chi_3) \mp \frac{s_{\pm}}{4m_b m_{\Lambda_b}} [(\chi_2 - \chi_4) \pm (\chi_5 - \chi_6)]. \quad (\text{A.11})$$

B Form Factor Parametrisation

The form factors for $\Lambda_b \rightarrow \Lambda$ transitions can be treated in a similar way as those for e.g. $B \rightarrow K^{(*)}$ transitions. To this end, one considers the analytic continuation into the complex t plane, where $q^2 = \text{Re}\{t\}$. For $0 \leq q^2 \leq t_-$ (semileptonic domain) the form factors describe the semileptonic decay region, $\Lambda_b \rightarrow \Lambda$. For $q^2 \geq t_+$ they describe the pair-production process $|0\rangle \rightarrow \bar{\Lambda}_b \Lambda$ (pair production domain). Here $t_{\pm} = (m_{\Lambda_b} \pm m_{\Lambda})^2$, and $|0\rangle$ denotes the hadronic vacuum.

Inbetween the two domains (i.e., for $t_- \leq q^2 \leq t_+$) exists a region where the unphysical process $\Lambda_b \rightarrow \Lambda H$ contributes. Here the *low-lying resonance* H with mass m_H denotes any hadron with one bottom quark and one strange anti-quark that fulfills

$$t_- < m_H^2 < t_+. \quad (\text{B.1})$$

A summary of these resonances and their spin-parity quantum numbers is given in table 2. The contribution of the corresponding poles in the complex plane can be included in the

parametrization of the form factors as follows (see e.g. [62, 63]),

$$f_\lambda^V(q^2) = \frac{f_\lambda^V(0)}{P(q^2, m_{B_s^*}(1^-))} \left[1 + b_1^{V,\lambda} (z(q^2, t_0) - z(0, t_0)) + \dots \right], \quad (\text{B.2})$$

$$f_\lambda^A(q^2) = \frac{f_\lambda^A(0)}{P(q^2, m_{B_s^*}(1^+))} \left[1 + b_1^{A,\lambda} (z(q^2, t_0) - z(0, t_0)) + \dots \right]. \quad (\text{B.3})$$

for $\lambda = 0, \perp$. Here the resonance factor is defined as

$$P(t, m_H^2) = 1 - \frac{t}{m_H^2}, \quad (\text{B.4})$$

and the remaining q^2 -dependence is obtained from a Taylor series in the variable

$$z(t, t_0) \equiv \frac{\sqrt{t_+ - t} - \sqrt{t_+ - t_0}}{\sqrt{t_+ - t} + \sqrt{t_+ - t_0}}, \quad (\text{B.5})$$

which corresponds to a conformal mapping of the complex t plane onto the unit disc $|z| \leq 1$. Given the currently available numerical precision for the form factors, it is sufficient to truncate the expansion after the first order. For the auxiliary parameter t_0 we choose $t_0 = 12 \text{ GeV}^2$.

C Statistical Analysis of the Transition Form Factors

This appendix is dedicated to details of our fit of the hadronic transition form factors. Specifically, we undertake the following steps.

- (a) The available lattice results [12] provide information on the HQET form factors ξ_1 and ξ_2 in the interval $q^2 \in [13.5, 20.5] \text{ GeV}^2$ (low recoil energy). This includes correlations between form-factor values at different values of q^2 which – non-surprisingly – are sizeable (up to $\simeq 100\%$ for form factors related to the same current at adjacent points). For a stable numerical analysis we therefore only consider the two q^2 values at the very boundaries of the simulated range which are expected to have minimal correlation.

To translate this into estimates for the helicity form factors $f_{\perp,0}^{V,A}(q^2)$, we allow for corrections to the HQET limit from subleading form factors $\chi_{n=1\dots 6}$, see appendix A. With no detailed information on the latter – following the principle of maximum entropy [64] – we use Gaussian priors, i.e. a normal distribution centered around zero with variance $\sigma = 1$ from naive power-counting. Notice that by construction this leads to prior distributions with flat q^2 -dependence.

The present lattice analysis do not provide correlation information between the two individual HQET form factors. Given the large correlations between individual q^2 points, we expect these correlations to be sizeable, too. As a consequence, we cannot completely determine the correlation between the data points for, say, the physical vector form factor. Notice that the correlation is further enhanced by the flat priors

for the subleading contributions χ_n . This issue can be solved as soon as improved lattice results for the physical form factors beyond the HQET limit will be available. The result of this part of the analysis is summarized in table 3. However, we find that the estimates correlations in excess of 97% lead to a degeneracy of the parameters in our fits. Hereafter, our incomplete estimates of the correlation between q^2 points are therefore disregarded.

q^2	f_{\perp}^V	f_0^V	f_{\perp}^A	f_0^A
13.5 GeV ²	0.73 ± 0.20	0.72 ± 0.21	0.48 ± 0.19	0.48 ± 0.19
20.5 GeV ²	1.40 ± 0.20	1.39 ± 0.21	0.85 ± 0.19	0.85 ± 0.19

Table 3. Estimates of mean values and standard deviations for helicity form factors $f_{\perp}^{V,A}$ and $f_0^{V,A}$, based on probability distributions obtained from lattice points [12] in the HQET limit and Gaussian priors for the subleading IW form factors. See text for details.

q^2	$R_{\perp}^{T,V}$	$R_0^{T,V}$	$R_{\perp}^{T5,A}$	$R_0^{T5,A}$
13.5 GeV ²	1.07 ± 0.45	1.10 ± 0.55	1.13 ± 0.66	1.12 ± 0.67
20.5 GeV ²	1.00 ± 0.19	1.03 ± 0.21	1.02 ± 0.30	1.03 ± 0.30
q^2 correlation	0.965	0.964	0.961	0.956
$a_{\lambda}^{\Gamma,\tilde{\Gamma}}$	1.205	1.235	1.342	1.294
$b_{\lambda}^{\Gamma,\tilde{\Gamma}} \cdot 10^2$	-1.00	-1.00	-1.57	-1.29
$c_{\lambda}^{\Gamma,\tilde{\Gamma}}$	5.01	5.74	4.51	4.61
$d_{\lambda}^{\Gamma,\tilde{\Gamma}}$	-0.195	-0.231	-0.171	-0.176
$\sigma_{\lambda}^{\Gamma,\tilde{\Gamma}}$	0.19	0.21	0.30	0.30

Table 4. Estimates of mean values and standard deviations for ratios of helicity form factors $R_{\lambda}^{\Gamma,\tilde{\Gamma}}$, based on probability distributions obtained from lattice points [12] in the HQET limit and Gaussian priors for the subleading IW form factors. See text for details.

- (b) As explained in the main text, the form factors for tensor and pseudotensor currents enter the observables in the form of *ratios* with the corresponding vector or axial-vector form factors. We therefore derive probability distributions for the ratios ($\lambda = 0, \perp, \Gamma = T, T5, \tilde{\Gamma} = V, A$)

$$R_{\lambda}^{\Gamma,\tilde{\Gamma}} \equiv \frac{f_{\lambda}^{\Gamma}}{f_{\lambda}^{\tilde{\Gamma}}}, \quad (\text{C.1})$$

again based on the lattice results [12] at the boundaries $q^2 = 13.5 \text{ GeV}^2$ and $q^2 = 20.5 \text{ GeV}^2$. In the heavy-quark limit these ratios are unity. Deviations are estimated by the same implementation of sub-leading corrections as described in (a).

The result of this part of the analysis is summarized in table 4.

Notice, that the ratios $R_\lambda^{\Gamma, \tilde{\Gamma}}$ are only very poorly constrained towards smaller values of q^2 . More precise inputs on these quantities directly from the lattice are desirable.

The high degree of correlation between q^2 points leads us to parametrize these ratios through linear interpolation in q^2 , and one random number r for their uncertainty.

We use

$$R_\lambda^{\Gamma, \tilde{\Gamma}}(q^2) = a_\lambda^{\Gamma, \tilde{\Gamma}} + b_\lambda^{\Gamma, \tilde{\Gamma}} q^2 + (c_\lambda^{\Gamma, \tilde{\Gamma}} + d_\lambda^{\Gamma, \tilde{\Gamma}} q^2) r_\lambda^{\Gamma, \tilde{\Gamma}} \quad (\text{C.2})$$

with fixed parameters $a_\lambda^{\Gamma, \tilde{\Gamma}}$ through $d_\lambda^{\Gamma, \tilde{\Gamma}}$ as given in table 4. In the above, $r_\lambda^{\Gamma, \tilde{\Gamma}} \sim \mathcal{N}(0, \sigma_\lambda^{\Gamma, \tilde{\Gamma}})$.

- (c) The above results can be continued to the low- q^2 region by taking into account information from sum-rule analyses (see e.g. [13, 65, 66]) to determine probability distributions for the helicity form factors $f_\perp^{V,A}(q^2 = 0)$ and $f_0^{V,A}(q^2 = 0)$ at maximal recoil. We have

$$f_{\perp,0}^{V(A)}(0) = C_{\perp,0} \xi_\Lambda(0) (1 \pm \zeta_{\perp,0}), \quad (\text{C.3})$$

where we describe the soft form factor by a normal distribution $\xi_\Lambda(0) \sim \mathcal{N}(\mu = 0.38, \sigma = 0.19)$ where, for concreteness, we have used the estimates from a SCET sum rule obtained in [13]. We further allow for two independent (ad-hoc) correction factors ζ_λ for the two helicities $\lambda = 0, \perp$ whose probability distributions are modelled as $\mathcal{N}(\mu = 0, \sigma = 0.25)$.

The helicity form factors at $q^2 = 0$ are to good approximation multivariate-normally distributed. The mean values and standard deviations read

$$f_\perp^V(0) = f_\perp^A(0) = 0.39 \pm 0.23, \quad f_0^V(0) = f_0^A(0) = 0.38 \pm 0.22. \quad (\text{C.4})$$

The form factors are strongly correlated, and we find for the correlation matrix

$$\rho^{\text{SSR}} = \left(\begin{array}{c|cccc} & f_\perp^V & f_\perp^A & f_0^V & f_0^A \\ \hline f_\perp^V & 1.00 & 0.56 & 0.77 & 0.78 \\ f_\perp^A & 0.56 & 1.00 & 0.77 & 0.77 \\ f_0^V & 0.77 & 0.77 & 1.00 & 0.53 \\ f_0^A & 0.78 & 0.77 & 0.53 & 1.00 \end{array} \right) \quad (\text{C.5})$$

Based on the inputs discussed above in points (a) and (c), we can now fit the helicity form factors for the vector and axial vector currents to our theory estimates. We use the parametrization given in eq. (B.2), which features two parameters $f_\lambda^\Gamma(0)$ and b_λ^Γ per form factor. The overall set of fit parameters therefore reads

$$\vec{x} \equiv (f_0^V(0), f_0^A(0), f_\perp^V(0), f_\perp^A(0), b_0^V, b_0^A, b_\perp^V, b_\perp^A). \quad (\text{C.6})$$

In our fit we use a uniform prior $P_0(\vec{x})$ that is supported on

$$0 \leq f_\lambda^\Gamma(0) \leq 1, \quad -60 \leq b_\lambda^\Gamma \leq +30, \quad (\text{C.7})$$

for all $\lambda = \perp, 0$ and $\Gamma = V, A$. The likelihood for the form factor estimates $P(\text{Estimates}|\vec{x})$ factorizes into

$$P(\text{Estimates}|\vec{x}) = P(\text{HQET}|\vec{x}) \times P(\text{SSR}|\vec{x}). \quad (\text{C.8})$$

The HQET components are

$$P(\text{HQET}|\vec{x}) = \prod_{\lambda=\perp,0}^{\Gamma=V,A} \mathcal{N}_2(\vec{\mu}^{\text{HQET},\Gamma,\lambda}, \Sigma^{\text{HQET},\Gamma,\lambda}; \vec{F}_\lambda^\Gamma(\vec{x})), \quad (\text{C.9})$$

where $\vec{\mu}^{\text{HQET},\Gamma,\lambda}$ and $\Sigma^{\text{HQET},\Gamma,\lambda}$ can be read off table 3, and \vec{F}_λ^Γ is an abbreviation for

$$\vec{F}_\lambda^\Gamma = (f_\lambda^\Gamma(13.5 \text{ GeV}^2; \vec{x}), f_\lambda^\Gamma(20.5 \text{ GeV}^2; \vec{x})). \quad (\text{C.10})$$

The SCET sum rule component reads

$$P(\text{SSR}|\vec{x}) = \mathcal{N}_4(\mu^{\text{SSR}}, \Sigma^{\text{SSR}}; \vec{F}(\vec{x})), \quad (\text{C.11})$$

where μ^{SSR} and Σ^{SSR} can be read off eq. (C.4) and eq. (C.5). In the above, we denote the form factor parametrization as

$$\vec{F}(\vec{x}) = (f_\perp^V(0; \vec{x}), f_\perp^A(0; \vec{x}), f_0^V(0; \vec{x}), f_0^A(0; \vec{x})). \quad (\text{C.12})$$

As usual the posterior $P(\vec{x}|\text{Estimates})$ follows from Bayes' theorem as

$$P(\vec{x}|\text{Estimates}) = \frac{P(\text{Estimates}|\vec{x})P_0(\vec{x})}{\int d\vec{x} P(\text{Estimates}|\vec{x})P_0(\vec{x})}. \quad (\text{C.13})$$

We find the best-fit point

$$\begin{aligned} \vec{x}^* &\equiv \arg \max P(\vec{x}|\text{Estimates}) \\ &= (0.33, 0.31, 0.34, 0.31, -1.75, -0.52, -1.58, -0.24). \end{aligned} \quad (\text{C.14})$$

This is a good fit, with the largest pull value being 0.05σ . We find $\chi^2 = 5.4 \cdot 10^{-3}$, and with $N_{\text{d.o.f.}} = 4$ degrees of freedom (from 12 observations reduced by 8 fit parameters) this yields a p value of > 0.99 .

D Details on the Kinematics

D.1 Λ_b Rest Frame

We define the momenta of the lepton pair (q) and the Λ -baryon (k) in the Λ_b -baryon rest frame (B-RF) as

$$q^\mu|_{\text{B-RF}} = (q^0, 0, 0, -|\vec{q}|), \quad k^\mu|_{\text{B-RF}} = ((m_{\Lambda_b} - q^0), 0, 0, +|\vec{q}|), \quad (\text{D.1})$$

i.e. the z -axis is along the flight direction of the Λ , and

$$q^0|_{\text{B-RF}} = \frac{m_{\Lambda_b}^2 - m_\Lambda^2 + q^2}{2m_{\Lambda_b}}, \quad |\vec{q}|_{\text{B-RF}} = \frac{\sqrt{\lambda(m_{\Lambda_b}^2, m_\Lambda^2, q^2)}}{2m_{\Lambda_b}}. \quad (\text{D.2})$$

D.2 Dilepton Rest Frame

The lepton angle θ_ℓ is defined as the angle between the ℓ^- direction of flight and the z -axis in the dilepton rest frame (2ℓ -RF) with the dilepton system decaying in the x - z -plane,

$$\begin{aligned} q_1^\mu|_{2\ell\text{-RF}} &= (E_\ell, -|\vec{q}_{2\ell\text{-RF}}| \sin \theta_\ell, 0, -|\vec{q}_{2\ell\text{-RF}}| \cos \theta_\ell), \\ q_2^\mu|_{2\ell\text{-RF}} &= (E_\ell, +|\vec{q}_{2\ell\text{-RF}}| \sin \theta_\ell, 0, +|\vec{q}_{2\ell\text{-RF}}| \cos \theta_\ell), \end{aligned} \quad (\text{D.3})$$

with

$$|\vec{q}_{2\ell\text{-RF}}|_{2\ell\text{-RF}} = \frac{\beta_\ell}{2} \sqrt{q^2}, \quad E_\ell|_{2\ell\text{-RF}} = \frac{\sqrt{q^2}}{2}, \quad \beta_\ell = \sqrt{1 - \frac{4m_\ell^2}{q^2}}. \quad (\text{D.4})$$

This implies

$$\bar{q}^\mu|_{2\ell\text{-RF}} = \sqrt{q^2} (0, -\beta_\ell \sin \theta_\ell, 0, -\beta_\ell \cos \theta_\ell). \quad (\text{D.5})$$

The various Lorentz scalars that can be built from the individual lepton momenta and the dilepton polarization vectors can then be written as

$$\begin{aligned} q_1 \cdot \varepsilon^{(*)}(0) &= -|\vec{q}_{2\ell\text{-RF}}| \cos \theta_\ell, & q_1 \cdot \varepsilon^{(*)}(\pm) &= \pm \frac{1}{\sqrt{2}} |\vec{q}_{2\ell\text{-RF}}| \sin \theta_\ell, \\ q_2 \cdot \varepsilon^{(*)}(0) &= +|\vec{q}_{2\ell\text{-RF}}| \cos \theta_\ell, & q_2 \cdot \varepsilon^{(*)}(\pm) &= \mp \frac{1}{\sqrt{2}} |\vec{q}_{2\ell\text{-RF}}| \sin \theta_\ell, \end{aligned} \quad (\text{D.6})$$

and

$$\begin{aligned} \varepsilon_{\mu\nu\rho\sigma} \varepsilon(0)^\mu \varepsilon(\pm)^\nu q_1^\rho q_2^\sigma &= +\frac{i}{\sqrt{2}} \sqrt{q^2} |\vec{q}_{2\ell\text{-RF}}| \sin \theta_\ell, \\ \varepsilon_{\mu\nu\rho\sigma} \varepsilon(+)^{\mu} \varepsilon(-)^{\nu} q_1^\rho q_2^\sigma &= +i \sqrt{q^2} |\vec{q}_{2\ell\text{-RF}}| \cos \theta_\ell, \end{aligned} \quad (\text{D.7})$$

and

$$\varepsilon_{\mu\nu\rho\sigma} \varepsilon(+)^{\mu} \varepsilon(-)^{\nu} \varepsilon(0)^\rho q_{1,2}^\sigma = +i \frac{\sqrt{q^2}}{2}. \quad (\text{D.8})$$

D.3 $N\pi$ System

The $N\pi$ system is characterized through its invariant mass $k^2 = m_\Lambda^2$, the angle θ_Λ between the N -direction of flight and the z -axis in the $N\pi$ rest frame ($N\pi$ -RF), and an azimuthal angle ϕ between the decay plane of the $N\pi$ system and the dilepton decay plane,

$$\begin{aligned} k_1^\mu|_{N\pi\text{-RF}} &= (E_N, -|\vec{k}_{N\pi\text{-RF}}| \sin \theta_\Lambda \cos \phi, -|\vec{k}_{N\pi\text{-RF}}| \sin \theta_\Lambda \sin \phi, +|\vec{k}_{N\pi\text{-RF}}| \cos \theta_\Lambda), \\ k_2^\mu|_{N\pi\text{-RF}} &= (E_\pi, +|\vec{k}_{N\pi\text{-RF}}| \sin \theta_\Lambda \cos \phi, +|\vec{k}_{N\pi\text{-RF}}| \sin \theta_\Lambda \sin \phi, -|\vec{k}_{N\pi\text{-RF}}| \cos \theta_\Lambda), \end{aligned} \quad (\text{D.9})$$

with

$$\begin{aligned} |\vec{k}_{N\pi\text{-RF}}| &= \frac{\sqrt{\lambda(k^2, m_N^2, m_\pi^2)}}{2\sqrt{k^2}} \equiv \frac{\beta_{N\pi}}{2} \sqrt{k^2}, & \beta_{N\pi} &= \sqrt{\lambda(1, m_N^2/k^2, m_\pi^2/k^2)}, \\ E_N &= \sqrt{m_N^2 + \frac{\beta_{N\pi}^2 k^2}{4}}, & E_\pi &= \sqrt{m_\pi^2 + \frac{\beta_{N\pi}^2 k^2}{4}}. \end{aligned} \quad (\text{D.10})$$

Our convention for the azimuthal angle ϕ is consistent with that of Krüger/Matias [17].

E Explicit Spinor Representations

In order to calculate the various helicity amplitudes, we have used explicit expressions for the Dirac spinors that characterize baryons with a given momentum

$$p^\mu = (p^0, |\vec{p}| \sin \theta \cos \phi, |\vec{p}| \sin \theta \sin \phi, |\vec{p}| \cos \theta), \quad (\text{E.1})$$

and spin orientation $s = \pm 1/2$ (defined in their respective rest frames), see e.g. [67]:

$$u(p, s = +1/2) = \frac{1}{\sqrt{2(p^0 + m)}} \begin{bmatrix} +(p^0 + m - |\vec{p}|) \cos(\theta/2) \\ +(p^0 + m - |\vec{p}|) \sin(\theta/2) \exp(+i\phi) \\ +(p^0 + m + |\vec{p}|) \cos(\theta/2) \\ +(p^0 + m + |\vec{p}|) \sin(\theta/2) \exp(+i\phi) \end{bmatrix}$$

$$u(p, s = -1/2) = \frac{1}{\sqrt{2(p^0 + m)}} \begin{bmatrix} -(p^0 + m + |\vec{p}|) \sin(\theta/2) \exp(-i\phi) \\ +(p^0 + m + |\vec{p}|) \cos(\theta/2) \\ -(p^0 + m - |\vec{p}|) \sin(\theta/2) \exp(-i\phi) \\ +(p^0 + m - |\vec{p}|) \cos(\theta/2) \end{bmatrix}. \quad (\text{E.2})$$

For the helicity amplitudes characterizing $\Lambda_b \rightarrow \Lambda$ transitions with scalar, pseudoscalar, vector or axialvector currents, we then obtain

$$\begin{aligned} \bar{u}(k, \pm 1/2) u(p, \pm 1/2) &= \sqrt{s_+}, & \bar{u}(k, \pm 1/2) u(p, \mp 1/2) &= 0, \\ \bar{u}(k, \pm 1/2) \gamma_5 u(p, \pm 1/2) &= \mp \sqrt{s_-}, & \bar{u}(k, \pm 1/2) \gamma_5 u(p, \mp 1/2) &= 0, \end{aligned} \quad (\text{E.3})$$

and

$$\begin{aligned} \bar{u}(k, \pm 1/2) \gamma^\mu u(p, \pm 1/2) &= (\sqrt{s_+}, 0, 0, \sqrt{s_-}), \\ \bar{u}(k, \pm 1/2) \gamma^\mu \gamma_5 u(p, \pm 1/2) &= \pm (\sqrt{s_-}, 0, 0, \sqrt{s_+}), \end{aligned} \quad (\text{E.4})$$

and

$$\begin{aligned} \bar{u}(k, \pm 1/2) \gamma^\mu u(p, \mp 1/2) &= \sqrt{2s_-} \varepsilon^\mu(\pm), \\ \bar{u}(k, \pm 1/2) \gamma^\mu \gamma_5 u(p, \mp 1/2) &= \mp \sqrt{2s_+} \varepsilon^\mu(\mp). \end{aligned} \quad (\text{E.5})$$

Here the kinematic functions s_\pm have been defined in eq. (3.8).

References

- [1] M. Artuso, D. Asner, P. Ball, E. Baracchini, G. Bell, et al., *B, D and K decays*, *Eur.Phys.J.* **C57** (2008) 309–492, [[arXiv:0801.1833](#)].
- [2] M. Antonelli, D. M. Asner, D. A. Bauer, T. G. Becher, M. Beneke, et al., *Flavor Physics in the Quark Sector*, *Phys.Rept.* **494** (2010) 197–414, [[arXiv:0907.5386](#)].
- [3] **LHCb Collaboration** Collaboration, R. Aaij et al., *Implications of LHCb measurements and future prospects*, *Eur.Phys.J.* **C73** (2013) 2373, [[arXiv:1208.3355](#)].
- [4] **BaBar Collaboration, Belle Collaboration** Collaboration, A. Bevan et al., *The Physics of the B Factories*, [[arXiv:1406.6311](#)].

- [5] **LHCb collaboration** Collaboration, R. Aaij et al., *Measurement of the differential branching fraction of the decay $\Lambda_b^0 \rightarrow \Lambda\mu^+\mu^-$* , *Phys.Lett.* **B725** (2013) 25, [[arXiv:1306.2577](#)].
- [6] G. Hiller and A. Kagan, *Probing for new physics in polarized Λ_b decays at the Z*, *Phys.Rev.* **D65** (2002) 074038, [[hep-ph/0108074](#)].
- [7] C.-H. Chen and C. Geng, *Baryonic rare decays of $\Lambda_b \rightarrow \Lambda\ell^+\ell^-$* , *Phys.Rev.* **D64** (2001) 074001, [[hep-ph/0106193](#)].
- [8] T. Aliev, K. Azizi, and M. Savci, *Analysis of the $\Lambda_b \rightarrow \Lambda\ell^+\ell^-$ decay in QCD*, *Phys.Rev.* **D81** (2010) 056006, [[arXiv:1001.0227](#)].
- [9] K. Azizi, S. Kartal, A. Olgun, and Z. Tavukoglu, *Analysis of the semileptonic $\Lambda_b \rightarrow \Lambda\ell^+\ell^-$ transition in the topcolor-assisted technicolor model*, *Phys.Rev.* **D88** (2013), no. 7 075007, [[arXiv:1307.3101](#)].
- [10] T. Gutsche, M. A. Ivanov, J. G. Körner, V. E. Lyubovitskij, and P. Santorelli, *Rare baryon decays $\Lambda_b \rightarrow \Lambda\ell^+\ell^-$ ($\ell = e, \mu, \tau$) and $\Lambda_b \rightarrow \Lambda\gamma$: differential and total rates, lepton- and hadron-side forward-backward asymmetries*, [arXiv:1301.3737](#).
- [11] W. Wang, *Factorization of Heavy-to-Light Baryonic Transitions in SCET*, *Phys.Lett.* **B708** (2012) 119–126, [[arXiv:1112.0237](#)].
- [12] W. Detmold, C.-J. D. Lin, S. Meinel, and M. Wingate, *$\Lambda_b \rightarrow \Lambda\ell^+\ell^-$ form factors and differential branching fraction from lattice QCD*, *Phys.Rev.* **D87** (2013), no. 7 074502, [[arXiv:1212.4827](#)].
- [13] T. Feldmann and M. W. Yip, *Form Factors for $\Lambda_b \rightarrow \Lambda$ Transitions in SCET*, *Phys.Rev.* **D85** (2012) [[arXiv:1111.1844](#)].
- [14] A. Ali, C. Hambrock, A. Y. Parkhomenko, and W. Wang, *Light-Cone Distribution Amplitudes of the Ground State Bottom Baryons in HQET*, *Eur.Phys.J.* **C73** (2013) 2302, [[arXiv:1212.3280](#)].
- [15] G. Bell, T. Feldmann, Y.-M. Wang, and M. W. Y. Yip, *Light-Cone Distribution Amplitudes for Heavy-Quark Hadrons*, *JHEP* **1311** (2013) 191, [[arXiv:1308.6114](#)].
- [16] V. Braun, S. Derkachov, and A. Manashov, *Integrability of the evolution equations for heavy-light baryon distribution amplitudes*, [arXiv:1406.0664](#).
- [17] F. Krüger and J. Matias, *Probing new physics via the transverse amplitudes of $B^0 \rightarrow K^{*0}(\rightarrow K^-\pi^+)\ell^+\ell^-$ at large recoil*, *Phys.Rev.* **D71** (2005) 094009, [[hep-ph/0502060](#)].
- [18] W. Altmannshofer, P. Ball, A. Bharucha, A. J. Buras, D. M. Straub, et al., *Symmetries and Asymmetries of $B \rightarrow K^*\mu^+\mu^-$ Decays in the Standard Model and Beyond*, *JHEP* **0901** (2009) 019, [[arXiv:0811.1214](#)].
- [19] C. Bobeth, G. Hiller, and G. Piranishvili, *CP Asymmetries in $\bar{B} \rightarrow \bar{K}^*(\rightarrow \bar{K}\pi)\bar{\ell}\ell$ and Untagged $\bar{B}_s, B_s \rightarrow \phi(\rightarrow K^+K^-)\bar{\ell}\ell$ Decays at NLO*, *JHEP* **0807** (2008) 106, [[arXiv:0805.2525](#)].
- [20] U. Egede, T. Hurth, J. Matias, M. Ramon, and W. Reece, *New observables in the decay mode $\bar{B}_d \rightarrow \bar{K}^{*0}\ell^+\ell^-$* , *JHEP* **0811** (2008) 032, [[arXiv:0807.2589](#)].
- [21] C. Bobeth, G. Hiller, and D. van Dyk, *The Benefits of $\bar{B} \rightarrow \bar{K}^*\ell^+\ell^-$ Decays at Low Recoil*, *JHEP* **1007** (2010) 098, [[arXiv:1006.5013](#)].

- [22] D. Becirevic and E. Schneider, *On transverse asymmetries in $B \rightarrow K^* \ell^+ \ell^-$* , *Nucl.Phys.* **B854** (2012) 321–339, [[arXiv:1106.3283](#)].
- [23] C. Bobeth, G. Hiller, and D. van Dyk, *General Analysis of $\bar{B} \rightarrow \bar{K}^{(*)} \ell^+ \ell^-$ Decays at Low Recoil*, *Phys.Rev.* **D87** (2013) 034016, [[arXiv:1212.2321](#)].
- [24] T. Mannel and S. Recksiegel, *Flavor changing neutral current decays of heavy baryons: The Case $\Lambda_b \rightarrow \Lambda \gamma$* , *J.Phys.* **G24** (1998) 979–990, [[hep-ph/9701399](#)].
- [25] T. Mannel and Y.-M. Wang, *Heavy-to-light baryonic form factors at large recoil*, *JHEP* **1112** (2011) 067, [[arXiv:1111.1849](#)].
- [26] **LHCb collaboration** Collaboration, R. Aaij et al., *Measurements of the $\Lambda_b^0 \rightarrow J/\psi \Lambda$ decay amplitudes and the Λ_b^0 polarisation in pp collisions at $\sqrt{s} = 7$ TeV*, *Physics Letters B* **724** (2013) 27, [[arXiv:1302.5578](#)].
- [27] G. Buchalla, A. J. Buras, and M. E. Lautenbacher, *Weak decays beyond leading logarithms*, *Rev.Mod.Phys.* **68** (1996) 1125–1144, [[hep-ph/9512380](#)].
- [28] K. G. Chetyrkin, M. Misiak, and M. Munz, *Weak radiative B meson decay beyond leading logarithms*, *Phys.Lett.* **B400** (1997) 206–219, [[hep-ph/9612313](#)].
- [29] A. J. Buras, *Climbing NLO and NNLO Summits of Weak Decays*, [arXiv:1102.5650](#).
- [30] M. Beneke, T. Feldmann, and D. Seidel, *Systematic approach to exclusive $B \rightarrow V \ell^+ \ell^-$, $V \gamma$ decays*, *Nucl.Phys.* **B612** (2001) 25–58, [[hep-ph/0106067](#)].
- [31] M. Beneke, T. Feldmann, and D. Seidel, *Exclusive radiative and electroweak $b \rightarrow d$ and $b \rightarrow s$ penguin decays at NLO*, *Eur.Phys.J.* **C41** (2005) 173–188, [[hep-ph/0412400](#)].
- [32] C. L. Lee, M. Lu, and M. B. Wise, *B_{14} and D_{14} decay*, *Phys.Rev.* **D46** (1992) 5040–5048.
- [33] A. Faessler, T. Gutsche, M. Ivanov, J. Korner, and V. E. Lyubovitskij, *The Exclusive rare decays $B \rightarrow K(K^*) \bar{\ell} \ell$ and $B_c \rightarrow D(D^*) \bar{\ell} \ell$ in a relativistic quark model*, *Eur.Phys.J.direct* **C4** (2002) 18, [[hep-ph/0205287](#)].
- [34] S. Faller, T. Feldmann, A. Khodjamirian, T. Mannel, and D. van Dyk, *Disentangling the Decay Observables in $B^- \rightarrow \pi^+ \pi^- \ell^- \bar{\nu}_\ell$* , *Phys.Rev.* **D89** (2014) 014015, [[arXiv:1310.6660](#)].
- [35] L. Okun, *Weak Interaction of Elementary Particles*. 1965.
- [36] C. Hambrock and G. Hiller, *Extracting $B \rightarrow K^*$ Form Factors from Data*, *Phys.Rev.Lett.* **109** (2012) 091802, [[arXiv:1204.4444](#)].
- [37] F. Beaujean, C. Bobeth, D. van Dyk, and C. Wacker, *Bayesian Fit of Exclusive $b \rightarrow \bar{s} \ell \ell$ Decays: The Standard Model Operator Basis*, *JHEP* **1208** (2012) 030, [[arXiv:1205.1838](#)].
- [38] C. Hambrock, G. Hiller, S. Schacht, and R. Zwicky, *$B \rightarrow K^*$ Form Factors from Flavor Data to QCD and Back*, *Phys.Rev.* **D89** (2014) 074014, [[arXiv:1308.4379](#)].
- [39] F. Beaujean, C. Bobeth, and D. van Dyk, *Comprehensive Bayesian Analysis of Rare (Semi)leptonic and Radiative B Decays*, [arXiv:1310.2478](#).
- [40] D. Das, G. Hiller, M. Jung, and A. Shires, *The $\bar{B} \rightarrow \bar{K} \pi \ell \ell$ and $\bar{B}_s \rightarrow \bar{K} K \ell \ell$ distributions at low hadronic recoil*, *JHEP* **1409** (2014) 109, [[arXiv:1406.6681](#)].
- [41] J. Charles, A. Le Yaouanc, L. Oliver, O. Pene, and J. Raynal, *Heavy to light form-factors in the heavy mass to large energy limit of QCD*, *Phys.Rev.* **D60** (1999) 014001, [[hep-ph/9812358](#)].

- [42] M. Beneke and T. Feldmann, *Symmetry breaking corrections to heavy to light B meson form-factors at large recoil*, *Nucl.Phys.* **B592** (2001) 3–34, [[hep-ph/0008255](#)].
- [43] C. W. Bauer, S. Fleming, D. Pirjol, and I. W. Stewart, *An Effective field theory for collinear and soft gluons: Heavy to light decays*, *Phys.Rev.* **D63** (2001) 114020, [[hep-ph/0011336](#)].
- [44] M. Beneke, A. Chapovsky, M. Diehl, and T. Feldmann, *Soft collinear effective theory and heavy to light currents beyond leading power*, *Nucl.Phys.* **B643** (2002) 431–476, [[hep-ph/0206152](#)].
- [45] H. Asatryan, H. Asatrian, C. Greub, and M. Walker, *Calculation of two loop virtual corrections to $b \rightarrow s\ell^+\ell^-$ in the standard model*, *Phys.Rev.* **D65** (2002) 074004, [[hep-ph/0109140](#)].
- [46] D. van Dyk et al., *EOS: A HEP Program for Flavor Observables*. The version used for this publication is available from <http://project.het.physik.tu-dortmund.de/source/eos/tag/lambdab>.
- [47] **UTfit Collaboration** Collaboration, M. Bona et al., *The Unitarity Triangle Fit in the Standard Model and Hadronic Parameters from Lattice QCD: A Reappraisal after the Measurements of Δm_s and $BR(B \rightarrow \tau\nu_\tau)$* , *JHEP* **0610** (2006) 081, [[hep-ph/0606167](#)]. We use the updated data from Summer 2013 (post-EPS13), as obtained from <http://www.utfit.org/UTfit/ResultsSummer2013PostEPS>.
- [48] **Particle Data Group** Collaboration, J. Beringer et al., *Review of Particle Physics (RPP)*, *Phys.Rev.* **D86** (2012) 010001.
- [49] **Heavy Flavor Averaging Group** Collaboration, Y. Amhis et al., *Averages of B-Hadron, C-Hadron, and tau-lepton properties as of early 2012*, [arXiv:1207.1158](#). We use the update prepared for the PDG 2014 Review of Particle Physics.
- [50] **LHCb collaboration** Collaboration, R. Aaij et al., *Precision measurement of the Λ_b^0 baryon lifetime*, *Phys.Rev.Lett.* **111** (2013) 102003, [[arXiv:1307.2476](#)].
- [51] **LHCb collaboration** Collaboration, R. Aaij et al., *Measurements of the B^+ , B^0 , B_s^0 meson and Λ_b^0 baryon lifetimes*, *JHEP* **1404** (2014) 114, [[arXiv:1402.2554](#)].
- [52] M. Beylich, G. Buchalla, and T. Feldmann, *Theory of $B \rightarrow K^{(*)}\ell^+\ell^-$ decays at high q^2 : OPE and quark-hadron duality*, *Eur.Phys.J.* **C71** (2011) 1635, [[arXiv:1101.5118](#)].
- [53] **LHCb collaboration** Collaboration, R. Aaij et al., *Observation of a resonance in $B^+ \rightarrow K^+\mu^+\mu^-$ decays at low recoil*, *Phys.Rev.Lett.* **111** (2013), no. 11 112003, [[arXiv:1307.7595](#)].
- [54] A. Khodjamirian, T. Mannel, A. Pivovarov, and Y.-M. Wang, *Charm-loop effect in $B \rightarrow K^{(*)}\ell^+\ell^-$ and $B \rightarrow K^*\gamma$* , *JHEP* **1009** (2010) 089, [[arXiv:1006.4945](#)].
- [55] A. Khodjamirian, T. Mannel, and Y. Wang, *$B \rightarrow K\ell^+\ell^-$ decay at large hadronic recoil*, *JHEP* **1302** (2013) 010, [[arXiv:1211.0234](#)].
- [56] J. Lyon and R. Zwicky, *Resonances gone topsy turvy - the charm of QCD or new physics in $b \rightarrow s\ell^+\ell^-$?*, [arXiv:1406.0566](#).
- [57] **LHCb collaboration** Collaboration, R. Aaij et al., *Measurement of Form-Factor-Independent Observables in the Decay $B^0 \rightarrow K^{*0}\mu^+\mu^-$* , *Phys.Rev.Lett.* **111** (2013), no. 19 191801, [[arXiv:1308.1707](#)].

- [58] S. Jäger and J. Martin Camalich, *On $B \rightarrow V\ell^+\ell^-$ at small dilepton invariant mass, power corrections, and new physics*, *JHEP* **1305** (2013) 043, [[arXiv:1212.2263](#)].
- [59] W. Altmannshofer and D. M. Straub, *New physics in $B \rightarrow K^*\mu\mu$?*, *Eur.Phys.J.* **C73** (2013), no. 12 2646, [[arXiv:1308.1501](#)].
- [60] S. Descotes-Genon, J. Matias, and J. Virto, *Understanding the $B \rightarrow K^*\mu^+\mu^-$ Anomaly*, *Phys.Rev.* **D88** (2013), no. 7 074002, [[arXiv:1307.5683](#)].
- [61] B. Grinstein and D. Pirjol, *Exclusive rare $B \rightarrow K^*\ell^+\ell^-$ decays at low recoil: Controlling the long-distance effects*, *Phys.Rev.* **D70** (2004) 114005, [[hep-ph/0404250](#)].
- [62] C. Bourrely, I. Caprini, and L. Lellouch, *Model-independent description of $B \rightarrow \pi\ell\bar{\nu}$ decays and a determination of $|V_{ub}|$* , *Phys.Rev.* **D79** (2009) 013008, [[arXiv:0807.2722](#)].
- [63] A. Khodjamirian, C. Klein, T. Mannel, and Y.-M. Wang, *Form Factors and Strong Couplings of Heavy Baryons from QCD Light-Cone Sum Rules*, *JHEP* **1109** (2011) 106, [[arXiv:1108.2971](#)].
- [64] E. Jaynes and G. Bretthorst, *Probability Theory: The Logic of Science*. Cambridge University Press, 2003.
- [65] Y.-M. Wang, Y. Li, and C.-D. Lu, *Rare Decays of $\Lambda_b \rightarrow \Lambda\gamma$ and $\Lambda_b \rightarrow \Lambda\ell^+\ell^-$ in the Light-cone Sum Rules*, *Eur.Phys.J.* **C59** (2009) 861–882, [[arXiv:0804.0648](#)].
- [66] Y.-M. Wang, Y.-L. Shen, and C.-D. Lu, *$\Lambda_b \rightarrow p, \Lambda$ transition form factors from QCD light-cone sum rules*, *Phys.Rev.* **D80** (2009) 074012, [[arXiv:0907.4008](#)].
- [67] H. E. Haber, *Spin formalism and applications to new physics searches*, in *21st Annual SLAC Summer Institute on Particle Physics: Spin structure in high energy processes*, 1994. [hep-ph/9405376](#).